Ferrous ions containing layered double hydroxides (LDH) nanosheet for drug delivery and antibacterial treatment

Author:
Zhang, Hao

Publication Date:
2021

DOI:
https://doi.org/10.26190/unsworks/22681

Welcome to the Research Alumni Portal, Hao Zhang!

You will be able to download the finalised version of all thesis submissions that were processed in GRIS here.

Please ensure to include the **completed declaration** (from the Declarations tab), your **completed Inclusion of Publications Statement** (from the Inclusion of Publications Statement tab) in the final version of your thesis that you submit to the Library.

Information on how to submit the final copies of your thesis to the Library is available in the completion email sent to you by the GRS.

Thesis submission for the degree of Master of Philosophy

Thesis Title and Abstract | Declarations | Inclusion of Publications Statement | Corrected Thesis and Responses

Thesis Title

Ferrous Ions Containing Layered Double Hydroxides (LDH) Nanosheet for Drug Delivery and Antibacterial Treatment

Thesis Abstract

Micro/nanoscaled particles represent a group of intelligent materials that can precisely and rapidly respond to biological microenvironments and improve therapeutic outcomes. In order to maximize biomedical application potentials, developing nanoscale particles that are able to catalyse in-situ substrates to address the biological problems is highly desired but still remains a critical challenge. Herein, a 2D nanosheet-based catalytic nanoparticles with enzyme mimicking behaviour is developed for enhanced drug delivery toward the tumour microenvironment as well as the antibacterial treatment. The nanoparticles are constructed via a facile one-pot method and exhibit ultrathin monolayer nanosheet morphology and could be further attaching drugs as cargo to fulfil the drug delivery task. The 2D structure of the LDHs allows high catalytic activity, leading to a responsive, sustained, and relatively high amount of substrate transformation. Herein, in this thesis, H_2O_2 was used as the model substrate to demonstrate the nanoparticles catalyzing ability, as well as the potential applications. The Ferrous ion-containing LDHs was tested for different medicinal purposes, tumour targeting drug deliveries and antibacterial treatment

Welcome to the Research Alumni Portal, Hao Zhang!

You will be able to download the finalised version of all thesis submissions that were processed in GRIS here.

Please ensure to include the **completed declaration** (from the Declarations tab), your **completed Inclusion of Publications Statement** (from the Inclusion of Publications Statement tab) in the final version of your thesis that you submit to the Library.

Information on how to submit the final copies of your thesis to the Library is available in the completion email sent to you by the GRS.

Thesis submission for the degree of Master of Philosophy

Thesis Title and Abstract | **Declarations** | Inclusion of Publications Statement | Corrected Thesis and Responses

ORIGINALITY STATEMENT

☑ I hereby declare that this submission is my own work and to the best of my knowledge it contains no materials previously published or written by another person, or substantial proportions of material which have been accepted for the award of any other degree or diploma at UNSW or any other educational institution, except where due acknowledgement is made in the thesis. Any contribution made to the research by others, with whom I have worked at UNSW or elsewhere, is explicitly acknowledged in the thesis. I also declare that the intellectual content of this thesis is the product of my own work, except to the extent that assistance from others in the project's design and conception or in style, presentation and linguistic expression is acknowledged.

COPYRIGHT STATEMENT

☑ I hereby grant the University of New South Wales or its agents a non-exclusive licence to archive and to make available (including to members of the public) my thesis or dissertation in whole or part in the University libraries in all forms of media, now or here after known. I acknowledge that I retain all intellectual property rights which subsist in my thesis or dissertation, such as copyright and patent rights, subject to applicable law. I also retain the right to use all or part of my thesis or dissertation in future works (such as articles or books).

For any substantial portions of copyright material used in this thesis, written permission for use has been obtained, or the copyright material is removed from the final public version of the thesis.

AUTHENTICITY STATEMENT

☑ I certify that the Library deposit digital copy is a direct equivalent of the final officially approved version of my thesis.

Welcome to the Research Alumni Portal, Hao Zhang!

You will be able to download the finalised version of all thesis submissions that were processed in GRIS here.

Please ensure to include the **completed declaration** (from the Declarations tab), your **completed Inclusion of Publications Statement** (from the Inclusion of Publications Statement tab) in the final version of your thesis that you submit to the Library.

Information on how to submit the final copies of your thesis to the Library is available in the completion email sent to you by the GRS.

Thesis submission for the degree of Master of Philosophy

Thesis Title and Abstract | Declarations | **Inclusion of Publications Statement** | Corrected Thesis and Responses

UNSW is supportive of candidates publishing their research results during their candidature as detailed in the UNSW Thesis Examination Procedure.

Publications can be used in the candidate's thesis in lieu of a Chapter provided:

- The candidate contributed **greater than 50%** of the content in the publication and are the "primary author", i.e. they were responsible primarily for the planning, execution and preparation of the work for publication.
- The candidate has obtained approval to include the publication in their thesis in lieu of a Chapter from their Supervisor and Postgraduate Coordinator.
- The publication is not subject to any obligations or contractual agreements with a third party that would constrain its inclusion in the thesis.

☑ The candidate has declared that **their thesis has publications - either published or submitted for publication - incorporated into it in lieu of a Chapter/s. Details of these publications are provided below.**.

Publication Details #1

Full Title:	Chemotaxis-driven 2D Nanosheet for Directional Drug Delivery Toward the Tumor Microenvironment
Authors:	Hao Zhang, Zhenbang Cao, Qianyi Zhang, Jiangtao Xu, Sung Lai Jimmy Yun, Kang Liang, Zi Gu
Journal or Book Name:	Small
Volume/Page Numbers:	Volume 16, Issue 44
Date Accepted/Published:	14/10/2020
Status:	published
The Candidate's Contribution to the Work:	Most of the experiments designing and conducting; data obtaining and analysis, manuscript writing
Location of the work in the thesis and/or how the work is incorporated in the thesis:	The published data is incorporated in chapter 3.

Candidate's Declaration

I confirm that where I have used a publication in lieu of a chapter, the listed publication(s) above meet(s) the requirements to be included in the thesis. I also declare that I have complied with the Thesis Examination Procedure.

Ferrous Ions Containing Layered Double Hydroxides (LDHs) Nanosheet for Drug Delivery and Antibacterial Treatment

Hao Zhang

A thesis in fulfillment of the requirements for the degree of

Master of Philosophy

School of Chemical Engineering

Faculty of Engineering

February 2021

ACKNOWLEDGEMENTS

I would like to express my gratitude to my primary supervisor, Dr. Zi (Sophia) Gu, who provided me with this honorable opportunity to work on this research project regarding the development of medical nanomaterials. I would like to thank her for her support and guidance on my research work as well as her patience to enlighten me when I was frustrated with either my life or work throughout my entire MPhil career. I would not have enjoyed my research life and learned so much if it were not for her support and mentorship. I would also like to thank my co-supervisor, Dr. Kang Liang, for his professional help when I needed him in my project. I would like to extend my gratitude to dear previous members in Gu's group, Dr. Zhenbang Cao, who helped me a lot and gave me suggestions about LDHs particles synthesis, especially at the beginning when I knew little in this field. Then I would like to thank Qianyi, He Zhang because they patiently taught me on using lab instruments, analytical software, or performing data analysis. In addition, I would like to mention Adel, Nicki, Koentadi, Jeff, Junwei, Zongzong who gave me a lot of mental support or technical support that outside off my fields. I am deeply grateful for the financial and mental support of my family. I can never have the chance to start this journey of studying at UNSW if it were not for them. Last but not least, I would like to thank my lover, Tammy, who has given me with mental supports and trusts, even though we could not meet face-to-face during my research journey.

Published paper that contributed to this thesis and described in Chapter 3

Zhang, H., Cao, Z., Zhang, Q., Xu, J., Yun, S.L.J., Liang, K. and Gu, Z., 2020. Chemotaxis-Driven 2D Nanosheet for Directional Drug Delivery toward the Tumor Microenvironment. Small, 16(44), p.2002732.

ABBRIVIATIONS

AFM	atomic force microscopy
DAPI	4′,6-diamidino-2-phenylindole
DI	deionized
DLS	dynamic light scattering
DOX	doxorubicin
EC	*Escherichia coli*
Fe-LDH	ferrous aluminum layered double hydroxides
FITC	fluorescein isothiocyanate
FTIR	Fourier-transform infrared spectroscopy
LB	lysogeny broth
Lyso	lysozyme
MCF-7	Michigan cancer foundation 7
Mg-LDH	magnesium-aluminum layered double hydroxides
MHB	Mueller Hinton broth
MIC	minimum inhibitory concentration
MOFs	metal-organic frameworks
MSD	mean square displacement
OD	optical density
PBS	phosphate buffered saline
PCS	photon correlation spectroscopy
PEG	dual phosphonic acid-polyethylene glycol diblock copolymer

SA	*Staphylococcus aureus*
SEM	scanning electron microscope
TEM	transmission electron microscope
TGA	thermal gravity analysis
XRD	X-ray crystallography
ZIFs	zeolitic imidazolate frameworks

TABLE OF CONTENTS

Chapter 1
Introduction

The developments of layered double hydroxides (LDHs) have been raising the attention in the nanomaterials area. LDHs-based nanocomposites are being developed to other forms by combining different nanomaterials or modifying nanomaterials with functional molecules. The LDHs possess attraction and unique properties, for example, LDHs can incorporate various metal and small molecule as a carrier; LDHs have a high level of biosafety, and it can be degraded in biological and environmental systems; and the microstructure of LDHs renders them fascinating properties such pH responsiveness, tunable layer number and structural defects.[1-4] Although numerous evidences have shown LDHs can be widely applied in biomedical, environmental remediation, energy storage and conversion, the enzyme-like properties *via* redox-catalysis of LDHs have been rarely investigated. Therefore, the aim of my thesis project is to develop a highly efficient, dual enzyme mimetic LDH nanosheet for two key biomedical applications (i.e., drug delivery and antibacterial application).

In the following chapter, there will be a review regarding LDHs synthesis methods, characterization techniques and the potential applications.

To our best knowledge, there were few reports that using high-catalyst performance, Fe (II) as the divalent ion to construct LDHs. To prove the feasibility of Fe-LDH, a stable and high catalyzing efficacy PEGylated Fe-LDH and how it becomes a nanomotor for anti-cancer therapy will be discussed in chapter 3. Specifically, a surfactant-like polymer, PEG was added during the Fe-LDH synthesis in order to improve the ferrous catalyzing abilities. The ferrous

ions decompose the hydrogen peroxide into oxygen and therefore transform the chemical energy to mechanical energy. Interestingly, a self-directed movement was accidentally found during conducting the experiments. After the further investigate, this special phenomenon was classified to chemotaxis behaviors. Taking this advantage, loading a model drug doxorubicin and to fight against MCF-7 cancer cells were attempted.

In chapter 4, the functions of PEG/Fe-LDH were further explored to the antibacterial treatment. Due to the innate nature of ferrous, the Fe-LDH was placed to bacterial- mimicked environment, supplemented with hydrogen peroxide in acidic area to investigate the antibacterial efficiency. While it has a certain extent effect on dealing with gram-negative bacteria, it has very limited effects on gram-positive because this type of bacteria has thick cell wall for protection. To solve this problem, lysozyme was attempted and successfully coated onto PEG/Fe-LDH. The new nanocomposite, Lyso@PEG/Fe-LDH antibacterial effect was studied. By comparting their separate treatments, the Lyso@PEG/Fe-LDH was expected to have better results regarding antibacterial efficacy.

Finally, chapter 5 concludes the contribution in this thesis work to the research field of Fe-LDH. Based on the outcomes of this work, the potential implement and possible direction for Fe-LDH is proposed.

Chapter 2
Literature Review

2.1 Layered Double Hydroxide (LDH) Structures and Synthesis

Generally, layered double hydroxide (LDH) expressed as following formula: $[M^{2+}_{1-x}M^{3+}(OH)_2](A^{n-})_{x/n}\cdot mH_2O$, where M^{2+} are divalent metal ions and M^{3+} are trivalent ions.[1-4] The x value usually between 0.2–0.33, which means the M^{2+}/M^{3+} molar ratio is 2.0–4.0 (Figure 2.1).[5]

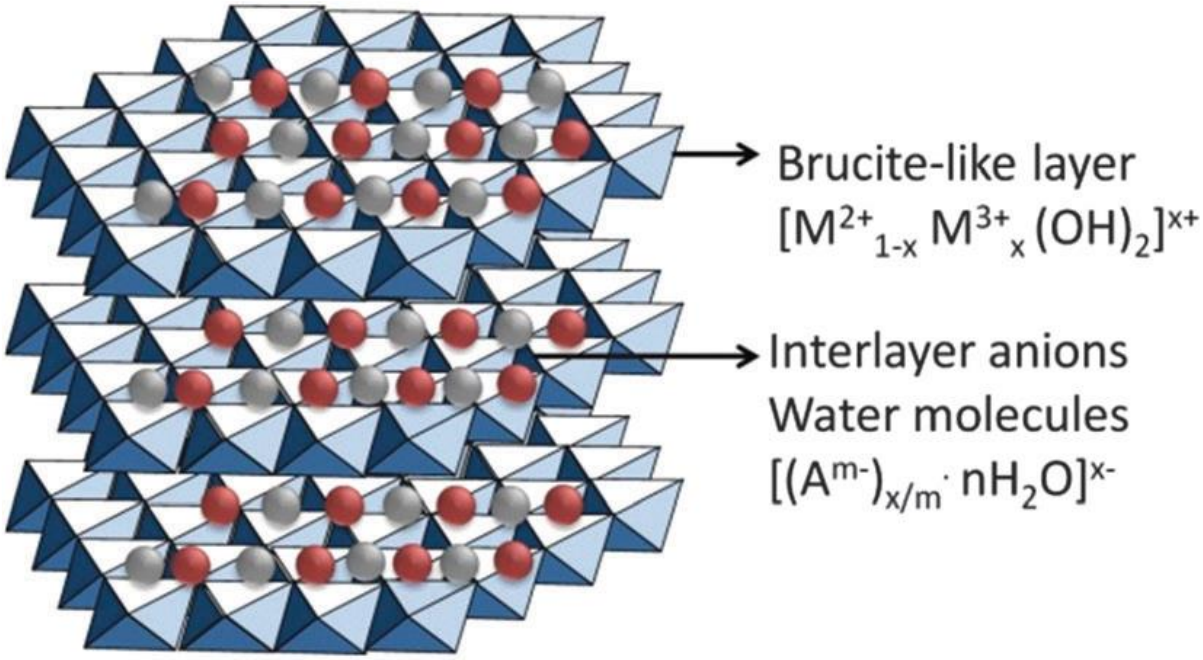

Figure 2.1. Schematic illustration of layered double hydroxide structure and chemical components.

For biomedical application, the divalent metal ions, in common, are Mg^{2+}, Fe^{2+}, Cu^{2+}, Mn^{2+}or Co^{2+} etc, while the trivalent ion could be Al^{3+}, Fe^{3+}, or Gd^{3+} etc. Also, the A^{n-} = Cl^-, CO_3^{2-}, NO_3^- and SO_4^{2-} etc. Xu et al (2015) examined the amorphous Al $(OH)_3$ and found that the Al $(OH)_3$ could re-precipitate on the LDH surface, blocking the further dissolvement and therefore increasing the LDH stability in the acidic aqueous solution.[6]

Traditional LDH has multilayered structure containing 5-20 brucite-like layers, and between

layers there is an interlayer space containing anions and water molecules. LDH can also be developed into few-layered and monolayered nanosheets. For the LDH nanosheet synthesis, typically, there are top-down and bottom-up routes to get the products.[7, 8] Top-down method refers to the concepts that separate the bulky materials to the tiny one. Exfoliation is one of top-down methods for synthesizing LDHs. Mao et al (2017) took the advantages of different charges of polymers and LDHs, successfully exfoliated the LDHs nanosheets *via* different polymers, resulting the thinner layers of the nanosheets (Figure 2.2).

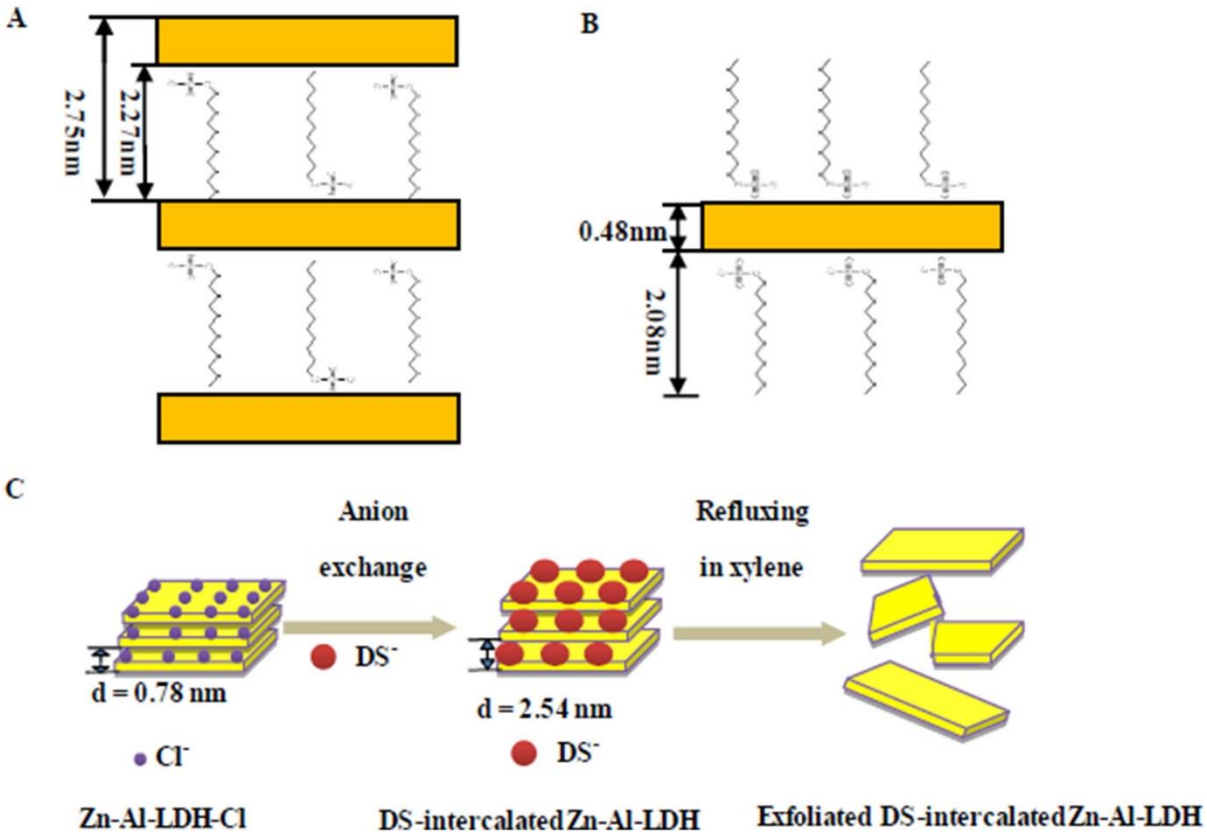

Figure 2.2. Schematic drawings of top-down route for synthesis LDHs nanosheets; dodecyl sulfate (DS) intercalated LDHs and its exfoliation process.

As for the bottom-up method, commonly speaking, it is ions crystallization on the crystal cores, or on other materials' surfaces. For instance, in order to harvest the energy from water droplets, Cui et al (2020) demonstrated the novel idea of fabricating the perpendicular LDHs on a 0.1m x 1 m large-scale aluminum foil, then, the LDHs were coated with other materials to improve the durance against acid and base. After the procedures, the composite was able to endure acid and based, thanks to the modified LDHs fabricating on the aluminum foil surface (Figure 2.3).

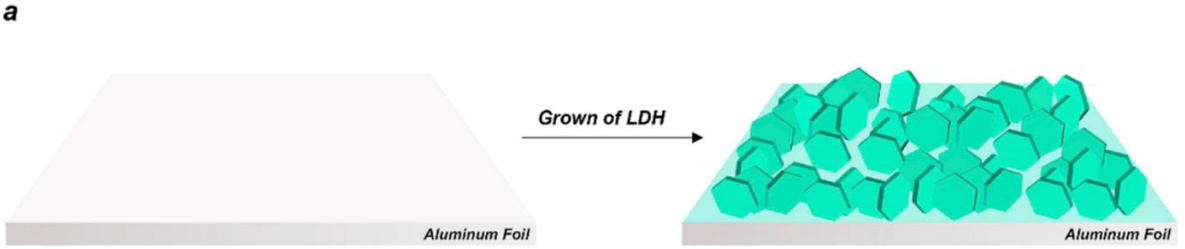

Figure 2.3. Schematic drawings of bottom-up route for synthesis LDHs nanosheets; in-situ grown of LDHs happened during the corrosion of the aluminum substrates resulting in perpendicularly formed LDHs.

Xu et al reported a facile but efficient bottom-up method for fabricating LDHs. Briefly, $MgCl_2$ and $AlCl_3$ (Molar ratio = 3:1) were dissolved and well mixed, then added into 0.006 mol NaOH under vigorous stirring, isolated from air and kept stirring for 30 mins. Then, the slurry was separated and washed *via* centrifuge. After that, re-dispersed the pellet and hydrothermally treated in an autoclave at 100 ^{o}C for 16h.

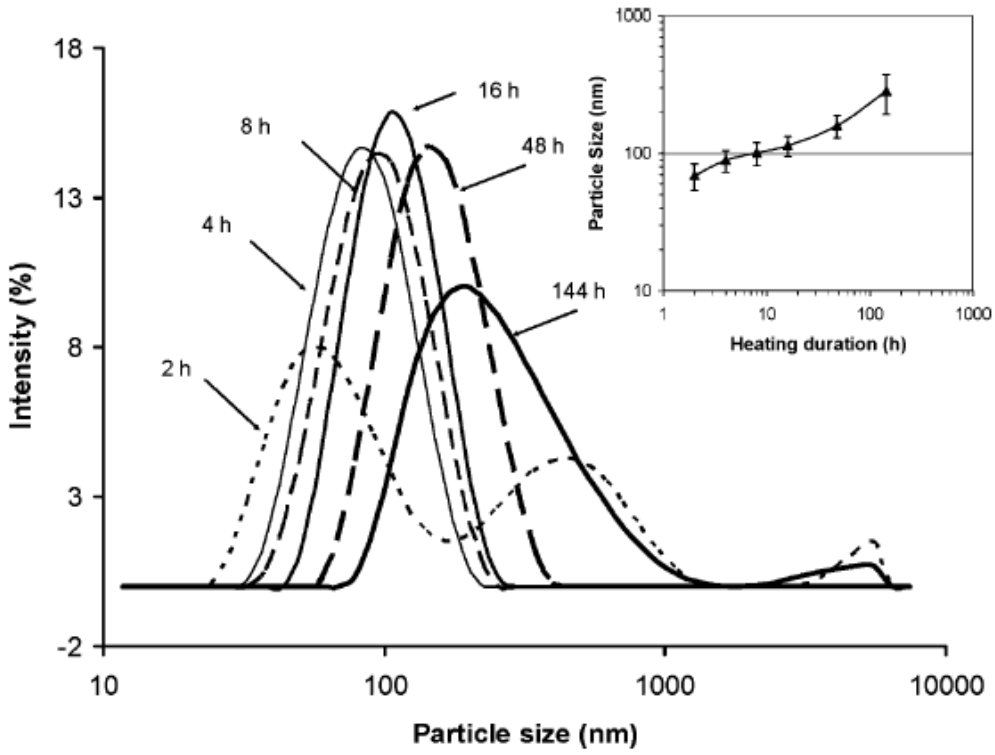

Figure 2.4. Particle size dispersion of Mg_2Al-Cl-LDH; aggregation happens during the hydrothermal treatment at 100 °C; the distribution curves were obtained with PCS[9].

By comparing with the conventional treatments, the as-prepared MgAl-LDH nanoparticles have small size around 60-150 nm (Figure 2.4), as well as narrow size distribution. They also characterized the MgAl-LDH nanoparticles by XRD and FTIR, both results demonstrate the as-prepared nanoparticle has typical patterns of MgAl-LDH structure. In addition, this method has been referenced to this project, Fe (II)-LDH synthesis.

2.2 LDHs catalyzing properties for enzyme-mimicking

Given the special structure of thin layer of these nanosheets, LDHs are the excellent materials and frequently used of catalyzing activities, due to the fact that there are numerous catalyzing sites could engage to the environment.[10-13]

A very recently paper, Iris et al (2019) compared the micro or macro/mesopore area on the LDH surface, which synthesized *via* different methods (urea hydrolysis, co-precipitation and aqueous miscible organic solvent (AMOST)) (Figure 2.5). By using these three different synthesis methods, they compared the LDH crystallite, size, hydrophilicity and accessibility, which may result in different catalyst performance.[14] They demonstrated the LDH as a heterogenous catalyst and successfully turned the glucose to fructose in the solution under 100 °C to 120 °C. The most fascinating point could be they did not use any surface modification method and successfully synthesized exfoliated layered double hydroxide.

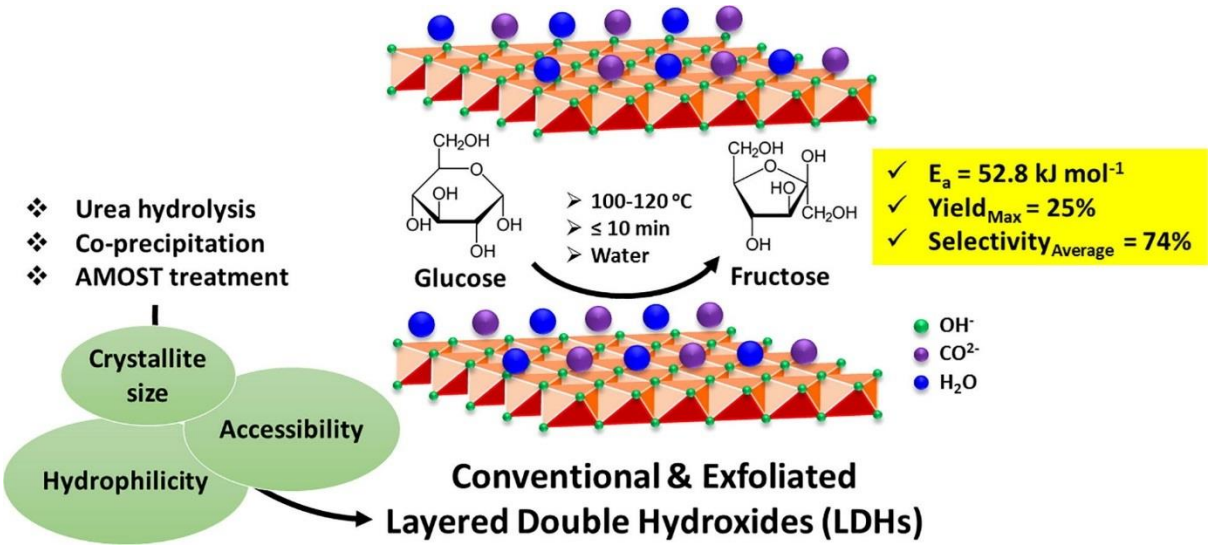

Figure 2.5. Schematic of catalyzing glucose to fructose by exfoliated layered double hydroxide.

Dou et al (2015) fabricated a nanocomposite that based on perpendicular LDHs and other 2D layered materials. They proposed that it is an efficient way to enhance the catalytic performance by taking advantage of the interfacial synergistic effects between the two materials; moreover, the strong coupling between LDHs and nanocarbon materials facilitates the charge transport at

the interface (i.e., improves the conductivity), which results to the high catalytic activity.[15] The examples illustrated above, are all relative to one important parameter, which is catalyst surface area. The reason why Dou et al (2015) constructed the upright LDHs on TiO_2 nanosphere surface is because the LDHs could have sufficient surface for engaging the liquid environment, and therefore increase the catalyst activities.

Some Iron (II) based layered double hydroxide can trigger Fenton reaction, which can be defined as the oxidation of organic substrates by iron (II) and hydrogen peroxide (Figure 2.6).

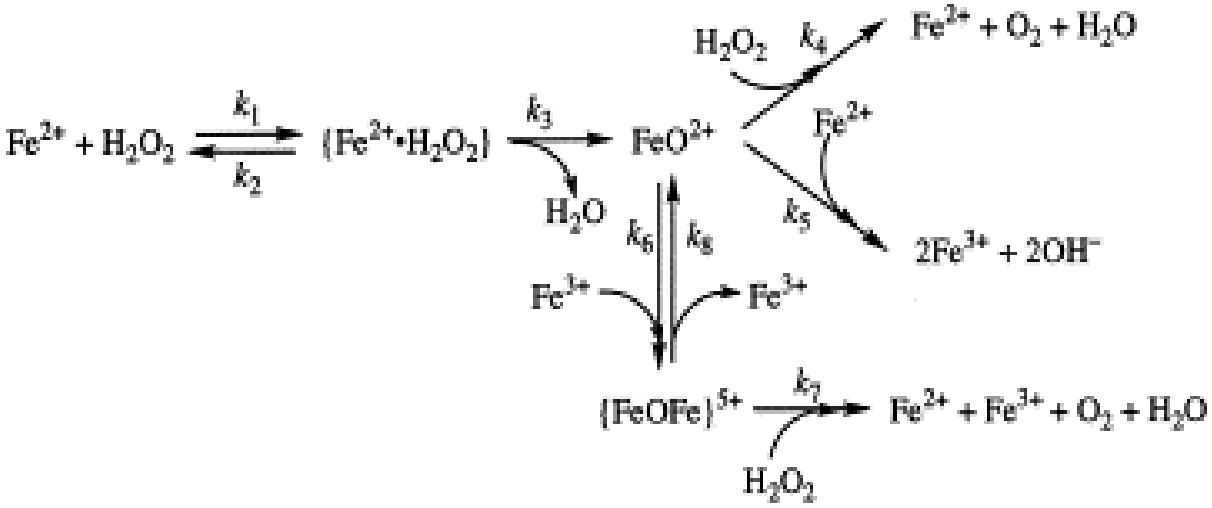

Figure 2.6. Schematic of Fenton reaction with Hydrogen peroxide.[16]

Implementing the Fenton reaction for biomedical applications is a novel mean due to the low cytotoxicity of the Iron element and less addition of chemical substrates. Chen et al (2012), they proposed an iron oxide nanoparticle for tumor therapies. The iron oxide nanoparticles (IONPs) have 'Enzyme-like' behaviors. When the IONPs come across with hydrogen peroxide, hydroxyl radicals are generated by hydrogen peroxide decomposition (Figure 2.8). [17]They quoted and summarized the mechanisms as follow (Figure 2.7):

$$Fe^{3+} + H_2O_2 \rightarrow FOOH^{2+} + H^+$$

$$FeOOH^{2+} \rightarrow Fe^{2+} + H^+ + O_2^-$$

$$Fe^{2+} + H_2O_2 \rightarrow Fe^{3+} + OH^- + OH\bullet$$

$$HO_2\bullet \rightarrow H^+ + O_2^-$$

$$OH\bullet + HO_2\bullet/O_2^- \rightarrow H_2O + O_2$$

Figure 2.7. Proposed mechanisms of Fe (III)- H_2O_2 reaction occurs through a radical-chain.[18]

Figure 2.8. Schematic illustration of the fabrication of TiO_2@CoAl-LDH core–shell nanospheres for oxygen evolution from water splitting

2.3 Enhancing Layered Double Hydroxides catalyzing ability

Enhancing LDHs catalyzing ability is in favor in the contemporary research works. Great efforts has been contributing to creating more defects or enriching LDHs surface areas.[19]

In order to enhance the LDHs catalyzing ability, Liu et al (2016) create a detects-rich LDHs and the modification leading to higher conversion rate of water to hydrogen and oxygen. They successfully delaminated and exfoliated the LDHs *via* DMF-ethanol solvent mixture (Figure 2.9). The product, CoFe LDH-F was reported that it has rich defects and outperform the conventional catalysts.[20]

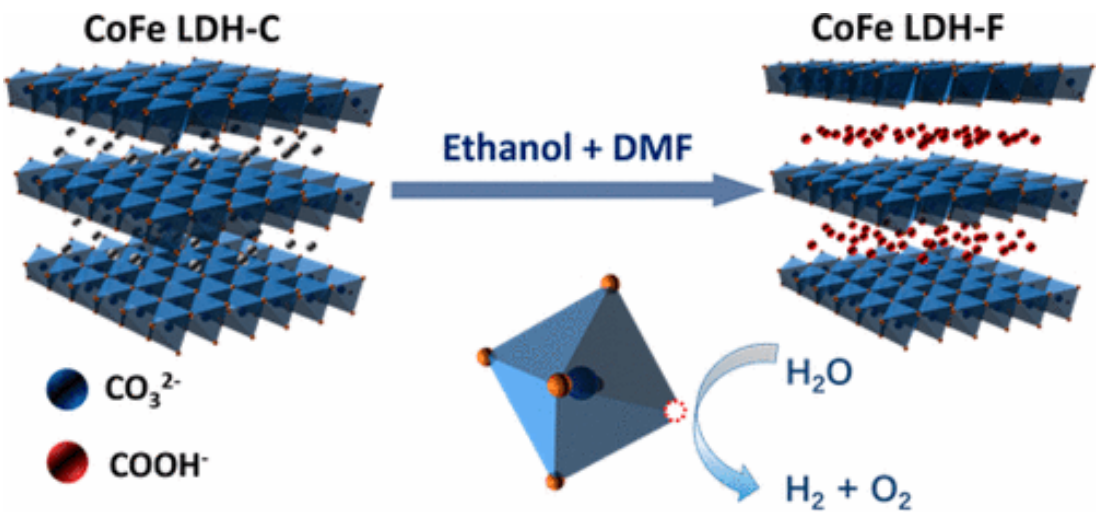

Figure 2.9. Schematic illustration of the fabrication of exfoliating CoFe LDHs *via* DMF-ethanol solvent mixture to construct defects-rich LDHs

Due to the exist of electrostatic repulsion, however, most of the two-dimensions materials, LDHs included, are easily aggregation.[21] The aggregation which could be covered the catalyzing sites on LDHs surface and hindering the LDHs to perform the catalyzing properties. Therefore, researchers have been developing new techniques for separating the LDH nanosheets from each other, such as, organic solvent, or conjugating DNA, functional proteins, surfactant-like polymers could separate the LDHs nanosheets from each other, making more surface area could be engaging other chemicals.[22]

Taking the advantages of positive charges on the LDH cation layers, the surface could be modified with some molecules through the molecules negative charge functional groups. It can be modified by inorganic, organic polymer or other forms of micro/macro- molecules (Figure 2.10).

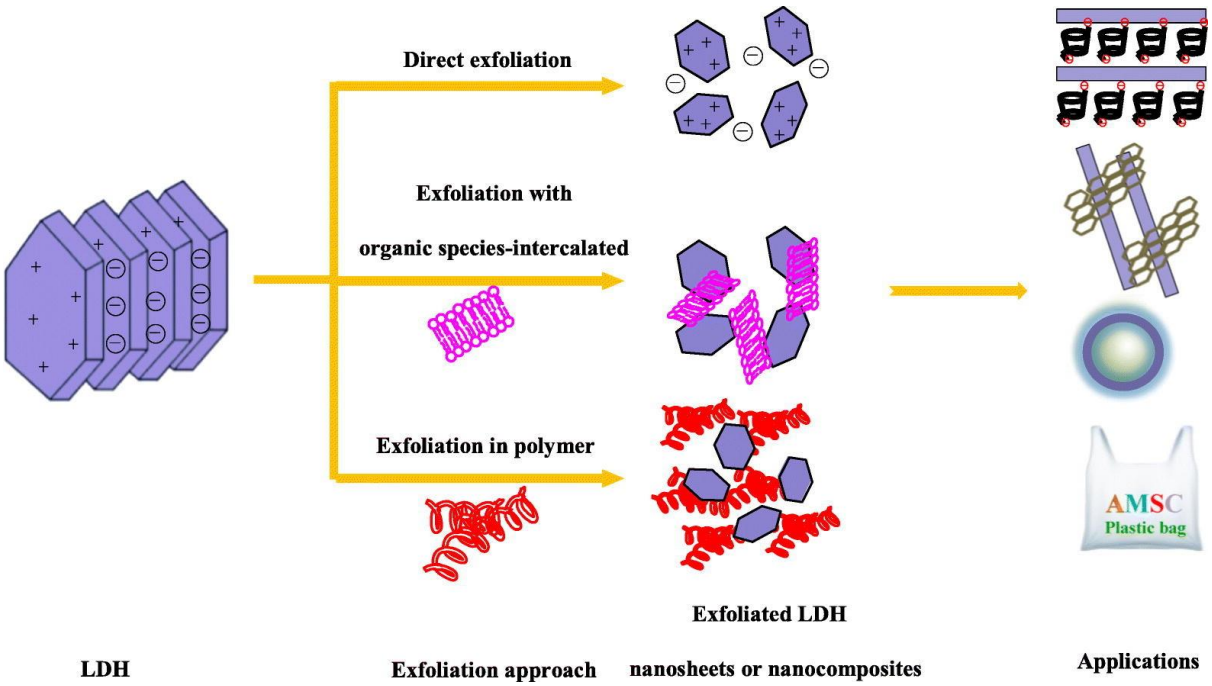

Figure 2.10. Schematic of LDHs exfoliation approaches

Gu et al (2015) successfully enhanced MgAl-LDH nanoparticles stability in cell culture and PBS by coating bovine serum albumin (BSA) on the positively charged LDH surface (Figure 2.11). They also point out that there are several factors could affect the BSA-LDH stability. Firstly, different sequences and the speed of reagent addition may end up with totally different results. Adding LDH nanoparticles suspension into BSA solution with high velocity results, or adding BSA solution into LDH suspension, both caused sever aggregation, which consists with the previous literature.[23] Secondly, the mass ratio of coating reagent verse LDH, which has the trend that the excessive of coating reagent could lead to smaller size of LDH nanoparticle. Thirdly, the LDH particles size, a fully comprehensive size-comparison indicates that, in the same mass ratio of BSA/LDH, the smaller size nanoparticles tend to have a larger extent size increase than the larger size nanoparticles.[24]

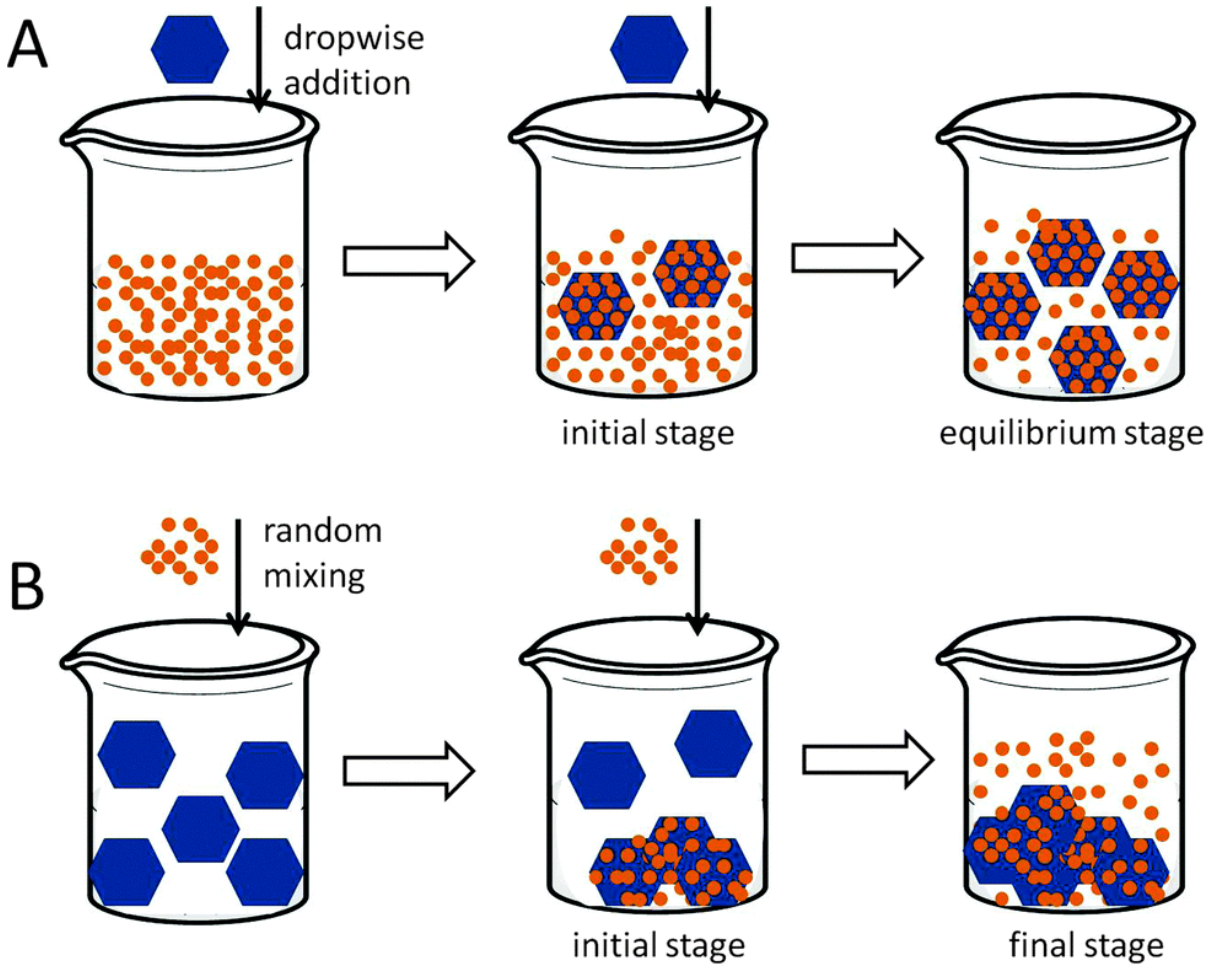

Figure 2.11. Schematic illustration of the BSA–LDH assembly process. (A) Dropwise addition of LDH suspension into BSA solution and (B) Random mixing of LDHs nanoparticles and BSA. Blue hexagonal plates: LDHs; and orange dots: BSA.

Cao et al (2018) reported that phosphonic acid terminated poly (ethylene glycol) (PEG) for LDH nanoparticle surfaces modification. They proposed two ways for conjugating PEG with LDH. For the first method, the metal salt solution was added to the base and then the precipitation was hydrothermally treated. After that, the PEG was added to the suspension after deprotonation (Figure 2.12). The mixture was then centrifuged to wash out unsaturated PEG.

Figure 2.12. Schematic illustration of organic acid deprotonation.

The second method was slightly different, the metal salt solution was added to strong base. Then the phosphate terminated PEG was added to the mixture and hydrothermally treated together. The two methods end up with different crystalline structures. PEG-LDH nanoparticles synthesis *via* the first method has completion of hexagonal structure while the second method ends up with deformed circle structure. (Figure 2.13). Meanwhile, from the TGA results, the PEG-LDH synthesis *via* second method end up with more PEG attained on the LDH surface (Figure 2.14).

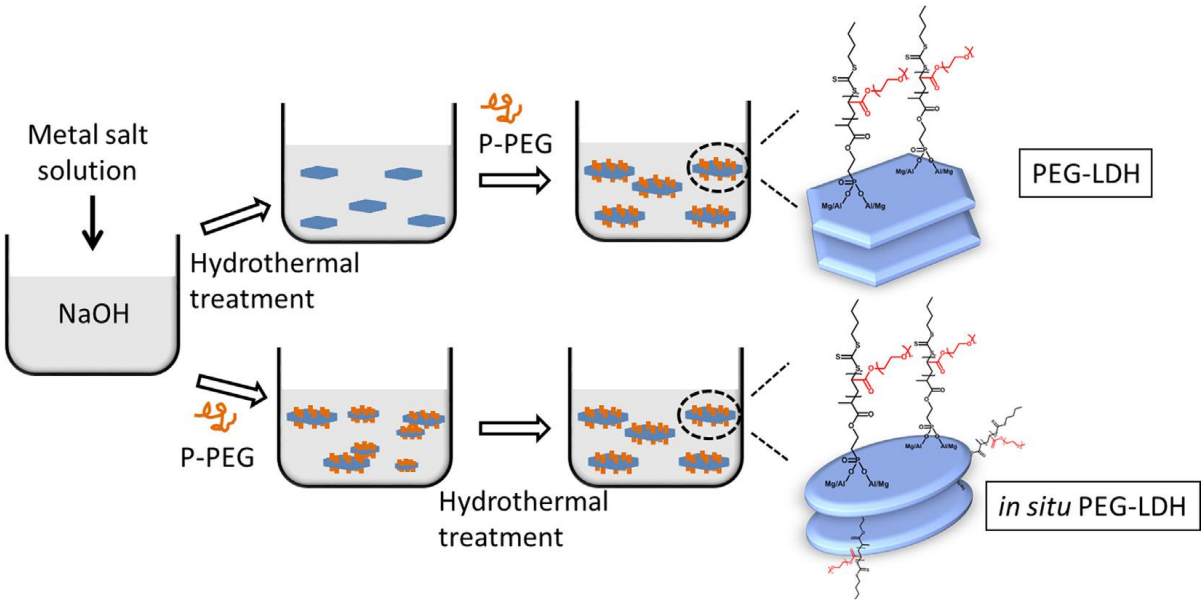

Figure 2.13. Proposed synthesis procedures of PEG-LDH and in situ PEG-LDH resulting in different PEG binding types. Metal salt solution was mixed with NaOH solution to form LDH nanoparticles, and P-PEG was added before and after LDH aging (hydrothermal treatment) to form in situ PEG-LDH and PEG-LDH respectively.[25]

2.4 Characterization techniques

As the surface modification was discussed above, there are two characterization methods for modifying LDHs with polymer worth to be mentioned.

Thermal gravity analysis (TGA)

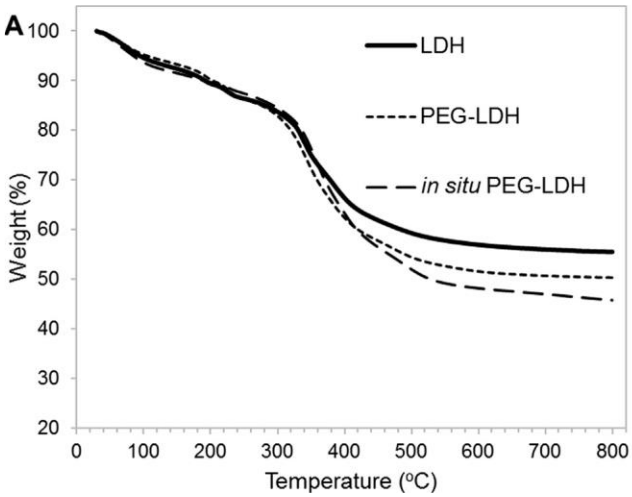

B	Weight Loss (%)	PEG content (%)
LDH	44.47	0
PEG-LDH	49.64	5.17
in situ PEG-LDH	54.18	9.71

Figure. 2.14. TGA weight-loss curves of LDH, PEG-LDH and in situ PEG-LDH (A) and table of weight loss (B) of LDH, PEG-LDH and in situ PEG-LDH.[25]

As their DLS results indicating that there are no significant differences between the sequence of the PEG addition, the conjugation comes more feasible for other materials uses. Most importantly, the PEG-LDH shows good stability in the electrolyte solution, as well as reduces non-specific protein adsorption on itself surface.

Fourier-transform infrared spectroscopy (FTIR)

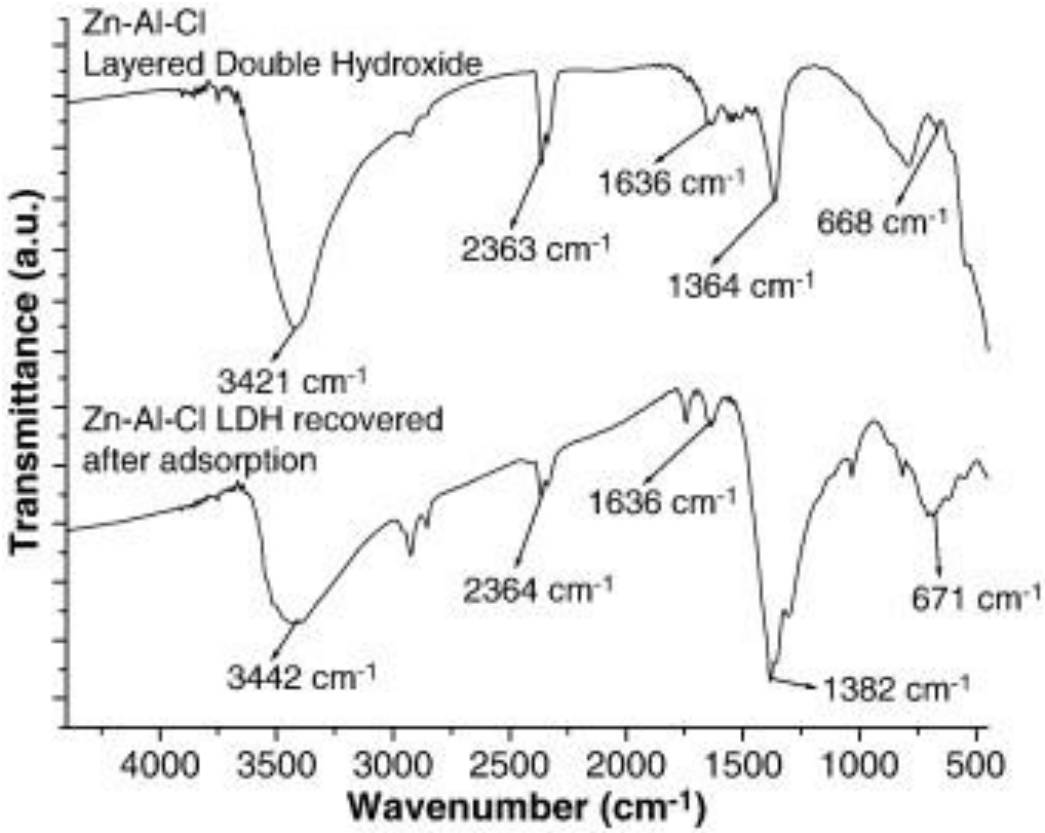

Figure 2.15. FTIR pattern of Zn–Al–Cl LDH and Zn–Al–Cl LDH recovered after nitrate adsorption [26].

A broad band occurs at 3421 cm^{-1} perhaps caused by superimposition of deformational vibrations of physically adsorbed water,[27] vibration of structural OH^- groups[28] and characteristic valent vibration of HO……OH in hydrotalcite.[29]

The band at 2363 cm^{-1} is related to CO_2 background of the measurement system.[30]

The band at 1636 cm^{-1} (bending vibration of δ H-O-H) may be assigned to the absorbed interlayer water. A band at 1364 cm^{-1} is because of the v3 stretching mode of carbonate ion, which might have formed due to the absorption of atmospheric CO_2 gas.[26]

The band at 668 cm^{-1} is probably due to M–O or O–M–O (In this case, M = Zn, Al)

vibrations.[31] Presence of nitrate group, which ascertains the adsorption of nitrate onto Zn–Al–Cl LDH is indicated by a band at 1382 cm^{-1}.[32] A broad band at 671 cm^{-1} is probably due to superposition of the characteristic bonds of hydrotalcite.

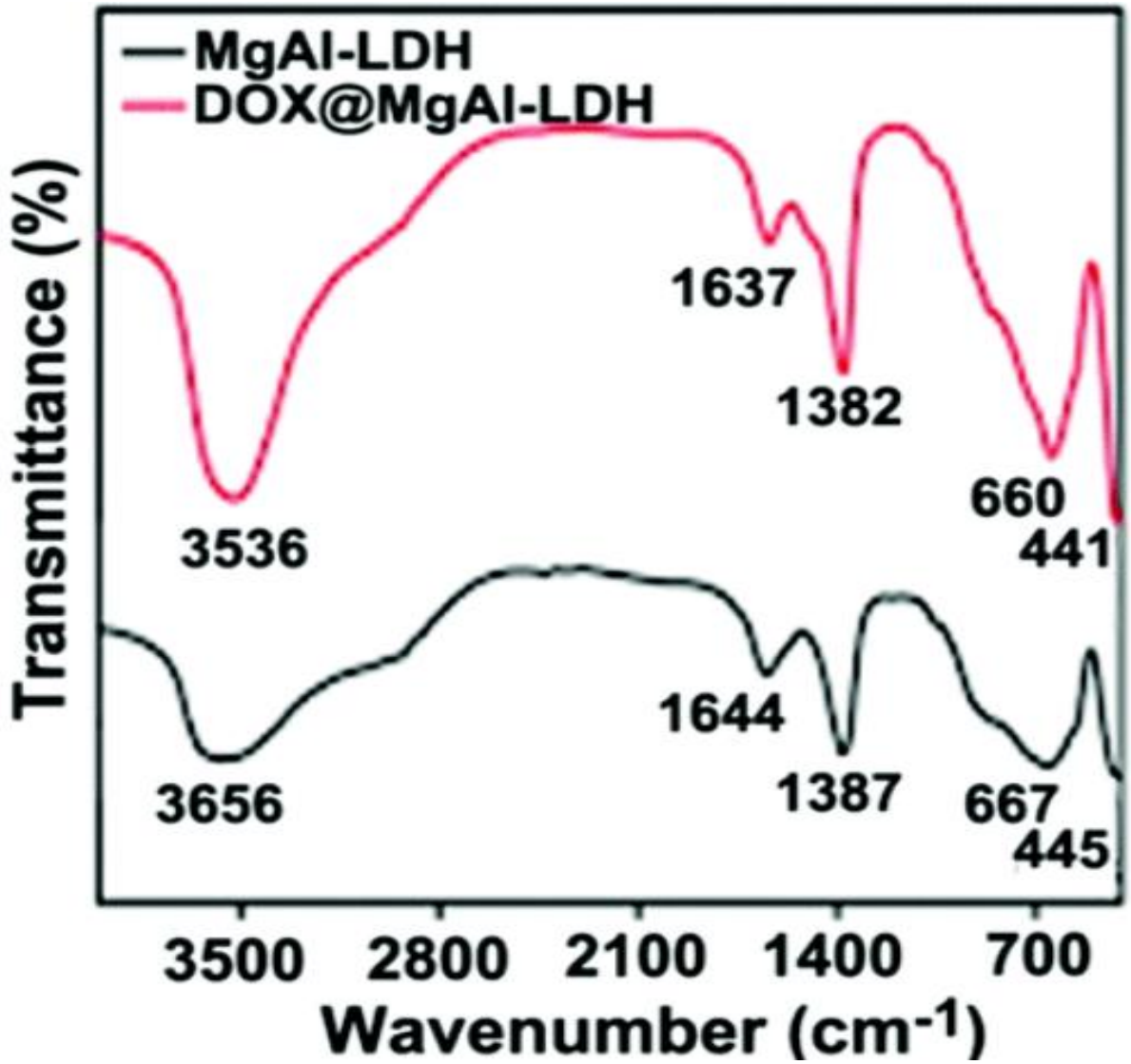

Figure. 2.16. FTIR spectra of MgAl-LDH and DOX@MgAl-LDH.[33]

The FTIR spectra of MgAl-LDH and DOX@MgAl-LDH have broad peaks in the range of 3360 - 3680 $cm^{-1}$and 1636-1367 cm^{-1} that be assigned to ν(OH) and δ (H_2O) groups. Peaks at 650 - 670 $cm^{-1}$and 410-446 can be assigned to M-O vibrations and M-O-H bending, where M stands for metals (In this case, M = Mg and Al) (Figure 2.16).[26]

In particular, the sharp peaks at 446 and 1352 cm^{-1}, double peaks at 769 and 661 cm^{-1} and a broad peak at 3396 cm^{-1} are all characteristic of LDH-based nanoparticles [34].

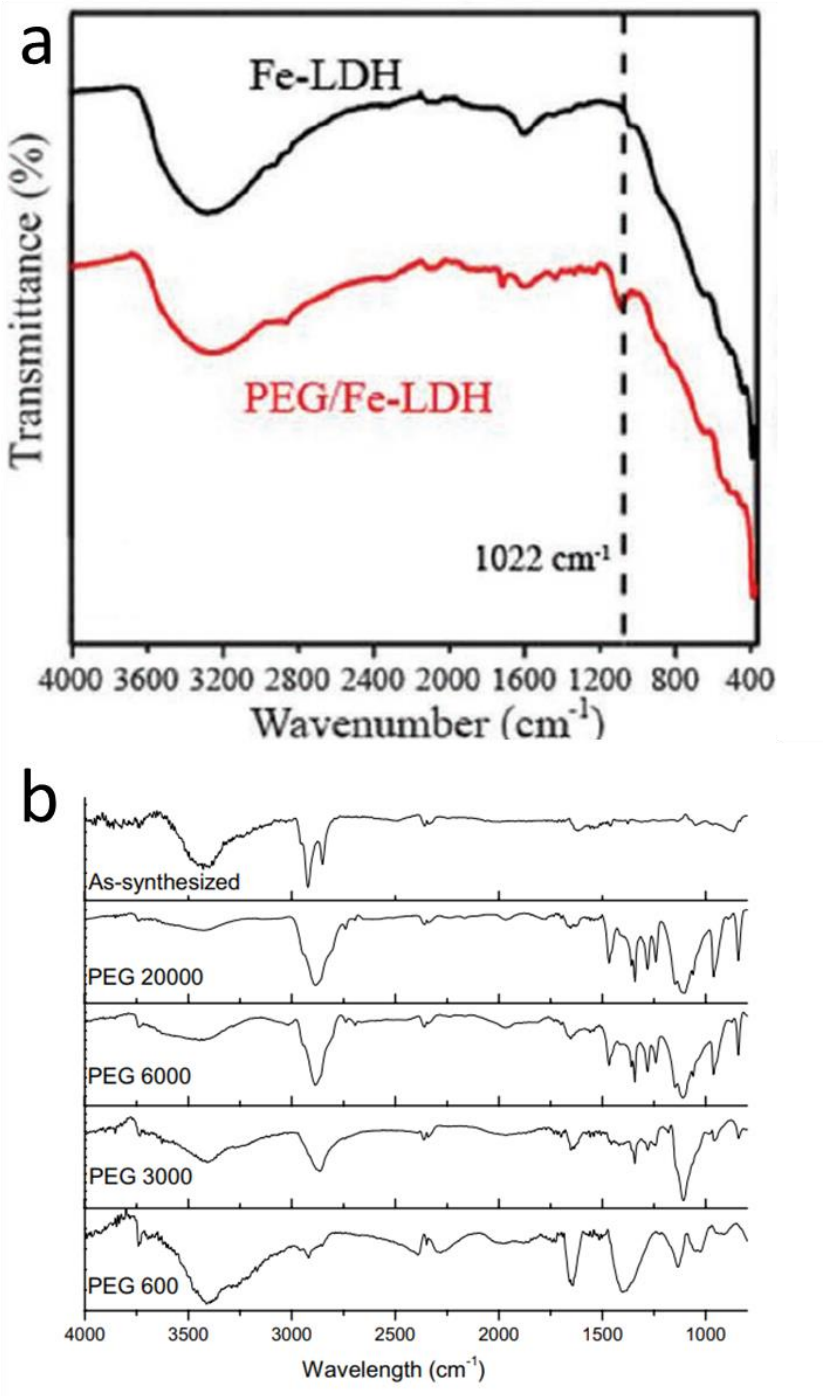

Figure 2.17. a) FTIR spectra of FeAl-LDH and PEG/FeAl-LDH.[35] b) IR study of the nanoparticles before and after modification with DPAPEG ligands.[36]

In comparison of spectrums before and after adding PEG, a new peak from (1250-1000 cm^{-1})

(Figure 2.17b) occurred due to the stretching vibration of C-O-C around 1100 cm^{-1} (Figure 2.17a), indicating the existent of PEGylation in the PEG/Fe-LDH, but not in the Fe-LDH spectrum.[36]

2.5 LDHs modification for specified purposes: drug delivery or medicinal treatments

Choy et al (2000) firstly reported that neutrally charged or positively charged LDH nanosheets have high efficiency in trapping anionic molecules, they successfully attached the LDH with negatively charged cell membranes and therefore expected an increase of bio-LDH uptake by a cell (Figure 2.18).[37] Similarly, Oh et al (2006) stated that the cell membrane coating-LDH can be taken up by cells *via* clathrin-mediated endocytosis (Figure 2.18).[38]

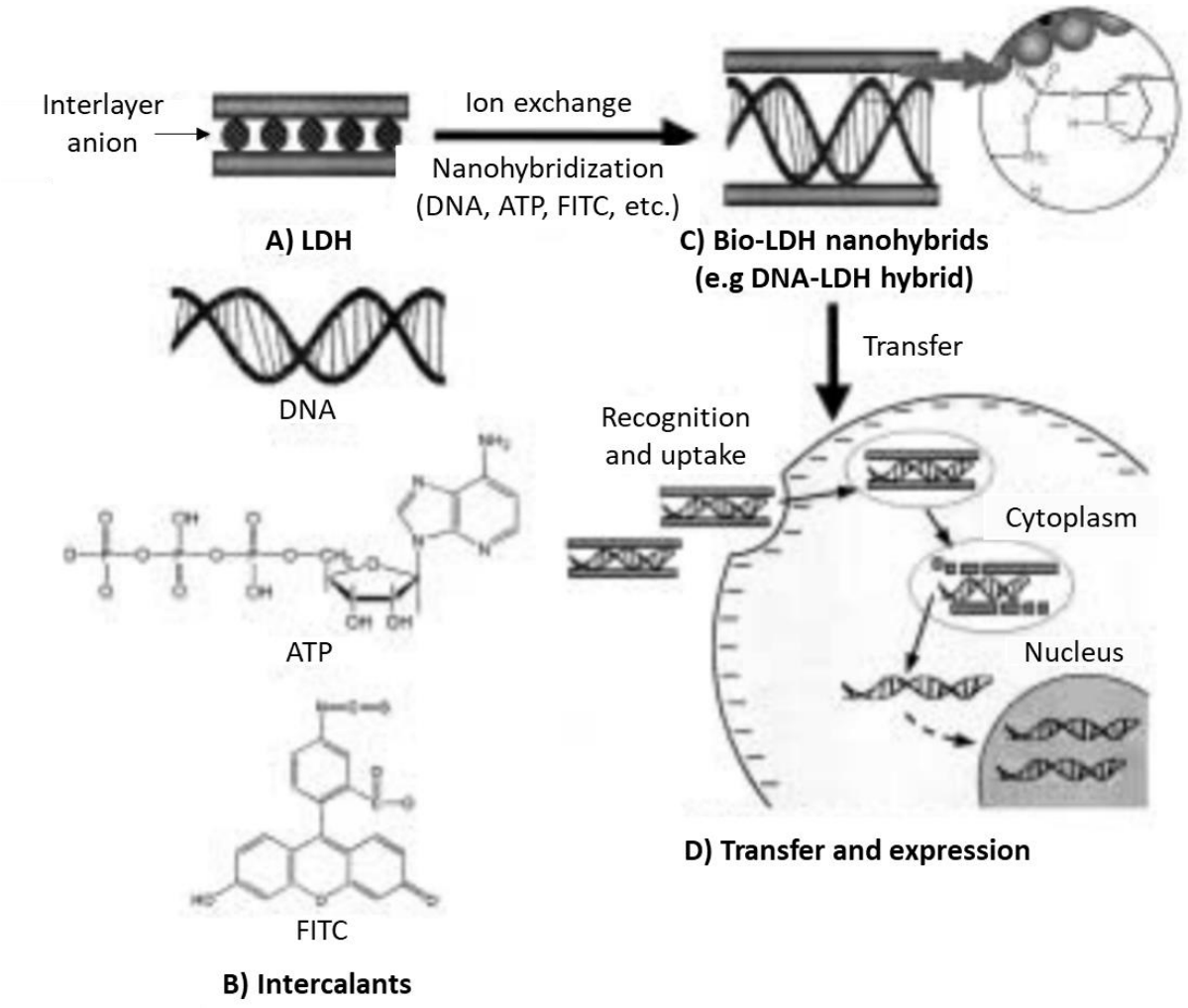

Figure 2.18 Schematic illustration of the dybridization and expected transfer mechanism of the bio-LDH hybrid into a cell.

Swadling et al (2013) reported the structure of RNA-LDH nanohybrid based on the computer simulation. They reveal that there was electrostatic attraction between the LDH surface and negative charged phosphate the RNA molecules, thus the bonding was form (Figure 2.19).[39] To be specific, the oxygen atoms on the phosphate group were contributing the lone pair electrons to the hydrogen atoms, which are from hydroxyl group on LDH metallic atoms. They also calculated that the bonding distance between the RNA and MgAl-LDH were calculated.

from 3.58 to 3.91 Å

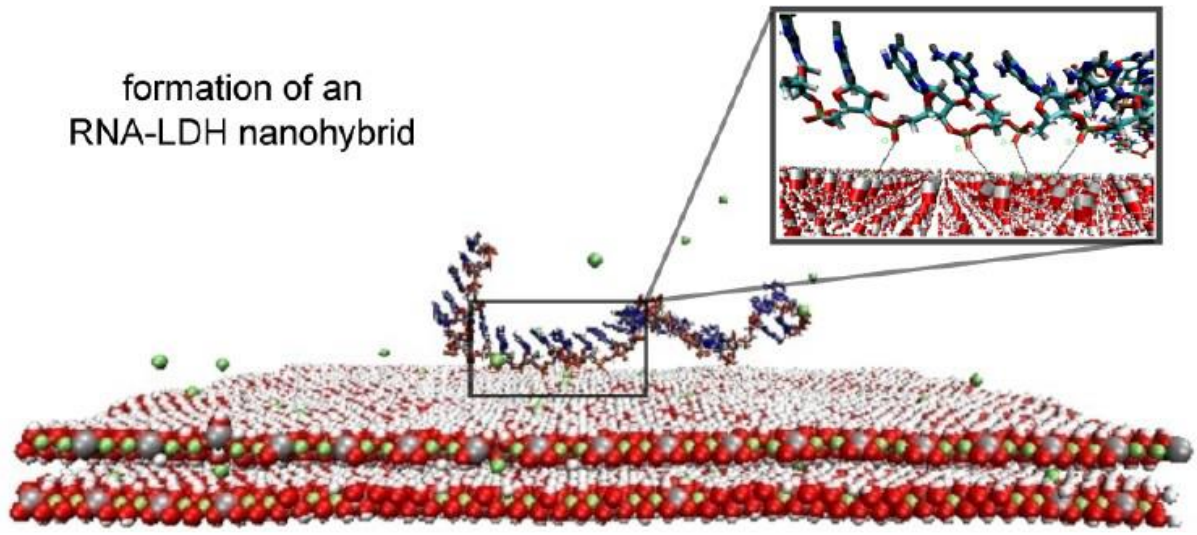

Figure 2.19. Schematic illustration of the formation of an RND-LDH nanohybrid

Some antitumor drugs have the side effects like, high toxicity and short half-time. Taking the advantageous property of special crystalline, layered double hydroxides has been reported as a competent vehicle that can achieve ‘loading drugs, delivering drugs and releasing drugs’ multiple tasks.

Xiao et al (2018) used MgAl-NO_3 to load 5- Fluorouracil(5-FU) by using the anion exchanging methods. It is well known that 5-FU can remarkably counter tumor activities. However, it also has the many side effects such as high toxicity and short half-time (Figure 2.20).

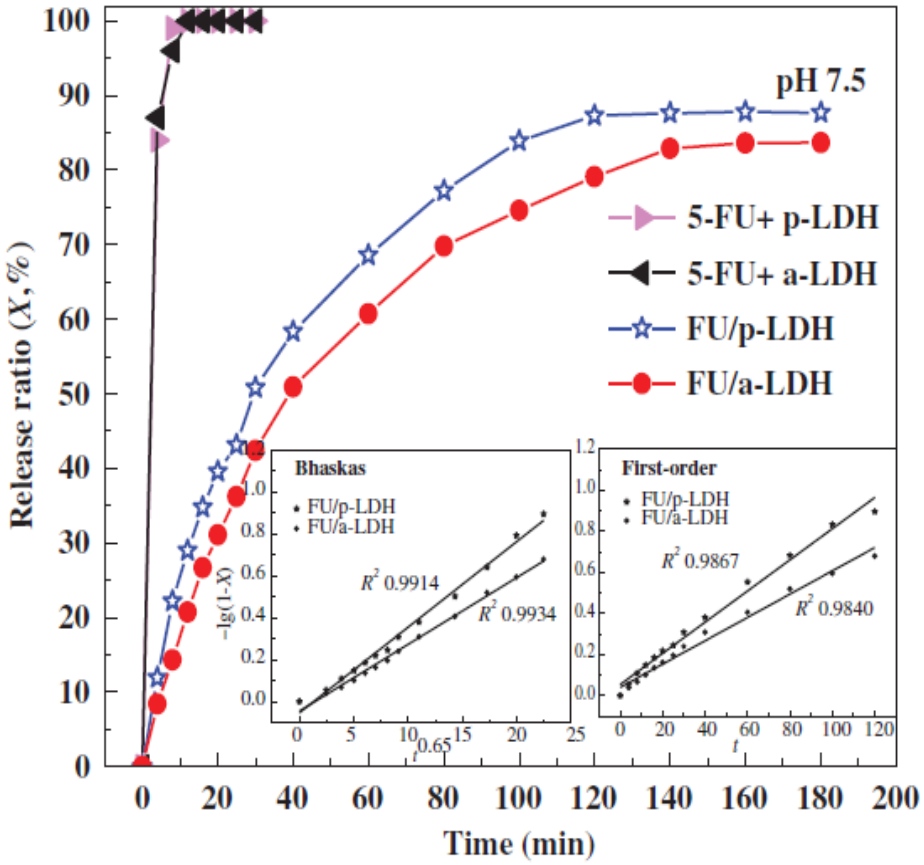

Figure 2.20. The release profile of 5-FU from the FU/a-LDH and FU/p-LDH composites in the PBS buffer (pH 7.5).[40]

They firstly pre-treated the MgAl-NO_3-LDH with $NaNO_3$-HNO_3 buffer solution to achieve a stable hydrotalcite structure, then add 5-FU: LDH (mass ratio of 4:1), with constant pH 10 and CO_2-free deionized water, string for 48h under N_2 atmosphere protection. The control release assay results show that the 5-FU and LDH physical mixtures has burst release in stimulated-gastrointestinal and intestinal environment while the 5-FU-LDH composite sustainably released.

Low molecular weight heparin (LMWH) is known as an effective anticoagulant, but it has pharmaceutical limitations such as short half-time (2-4h). Gu et al (2007) intercalated LMWH

(approximate 4 to 6 kD) into MgAl-Cl-LDH nanoparticles and had achieved extraordinary sustainable profile releases (Figure 2.21).

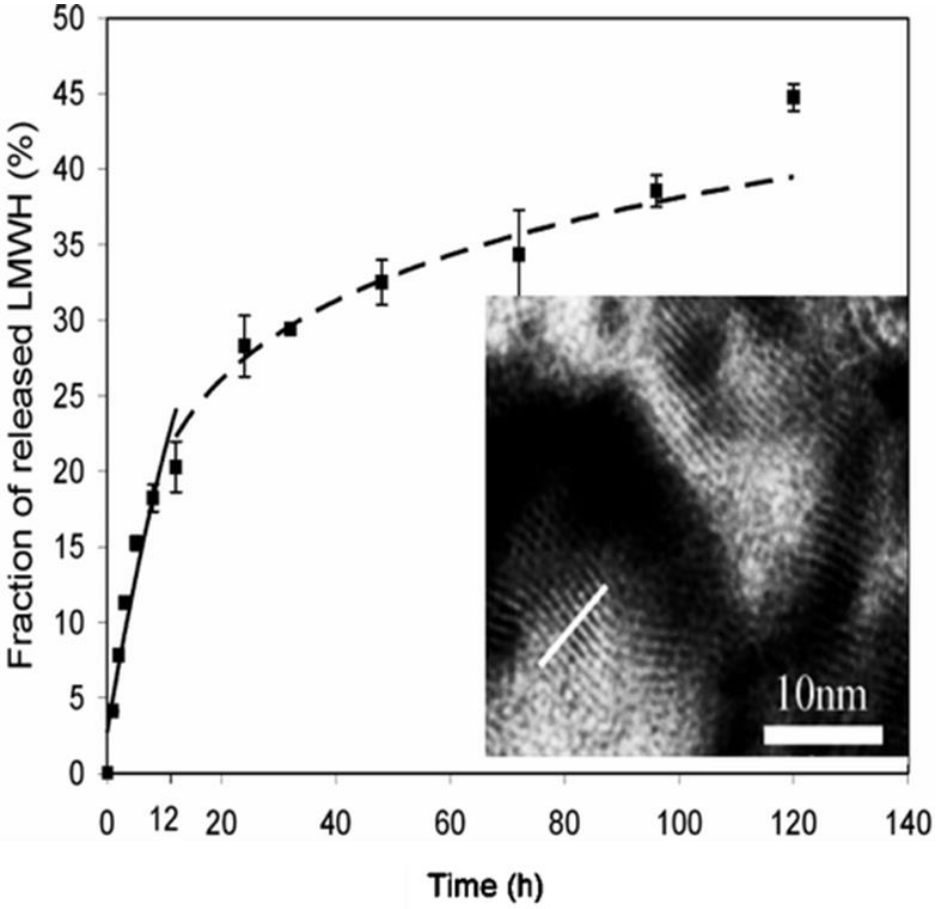

Figure 2.21. Two stages of in vitro LMWH release curves from LMWH20-LDH, within TEM images of LMWH20-LDH, X-axis: time (h) [41]

Gu et al also explained that the significant LMWH release extension is owing to the strong electrostatic interaction. To be specific, the positively charged LDH hydroxide layers interact with the negative charged LMWH anion in the LDH interlayer. This indicates that the drug release time intercalated in LDH nanoparticles, could have positive correlation with the number of multianionic species within the drug molecules.

In general, there are four dissolution-diffusion kinetic models can be used to fit the in vitro LMWH-LDH release:

(1) Zero-order model:

$$M_t - M_0 = -k_0 t$$

(2) First-order model:

$$\log (M_t/M_0) = - k_1 t$$

(3) The parabolic diffusion model:

$$(1 - M_t/M_0)/t) = k_d t^{-0.5} + a$$

(4) The modified Freundlich model:

$$(M_0 - M_t)/M_0 = k_m t^b$$

M_0 and M_t are the quantity of LMWH in the LDH hybrid at release time 0 and t; k the corresponding release rate constant; however, a and b constants whose chemical significance is not clearly resolved.

In Gu's work, stage I and II for LMWH20-LDH are best fitted with the modified Freundlich model, while the LMWH100-LDH are best fitted with parabolic diffusion model, with a linear correlation coefficient of R^2 = 0.95-0.99. In stage I, there is approximate 10-20% of LMWH on the LDH surface or at the edge of the nanoparticles, which tent to diffuse into the aqueous solution by exchanging with PO_3^- and Cl^-. Meanwhile, the LMWH within LDH interlayer diffuses toward to the edges and surfaces along with the leaking of magnesium cations as well as the dissolution of LDH hydrotalcite structure, together resulting in continuous release of LMWH from LDH. This consistent with, Yang et al (2007) previously detailed explanation about the two models; the modified Freundlich model describes heterogeneous diffusion from

the flat surfaces *via* ion exchanges, but the parabolic diffusion model describes the intraparticle diffusion or surface diffusion.[42]

Similarly, Huang et al (2017) intercalated a clinically approved chemotherapeutic drug methotrexate (MTX) into MnFe-LDH and achieve excellent pH-responsive drug releasing control. (From Figure 2.22)

Huang et al analyzed the XRD results, they found that the LDH interspacing increased after loading the MTX, indicating the drug molecules were successfully intercalated. From the DLS results, the MnFe-MTX-LDH hydrodynamic diameter remains around 49 nm after over 8 days aging, indicating the good stability. Also, from the TEM images, they claimed that there are no significant morphological changes between before and after loading MTX.

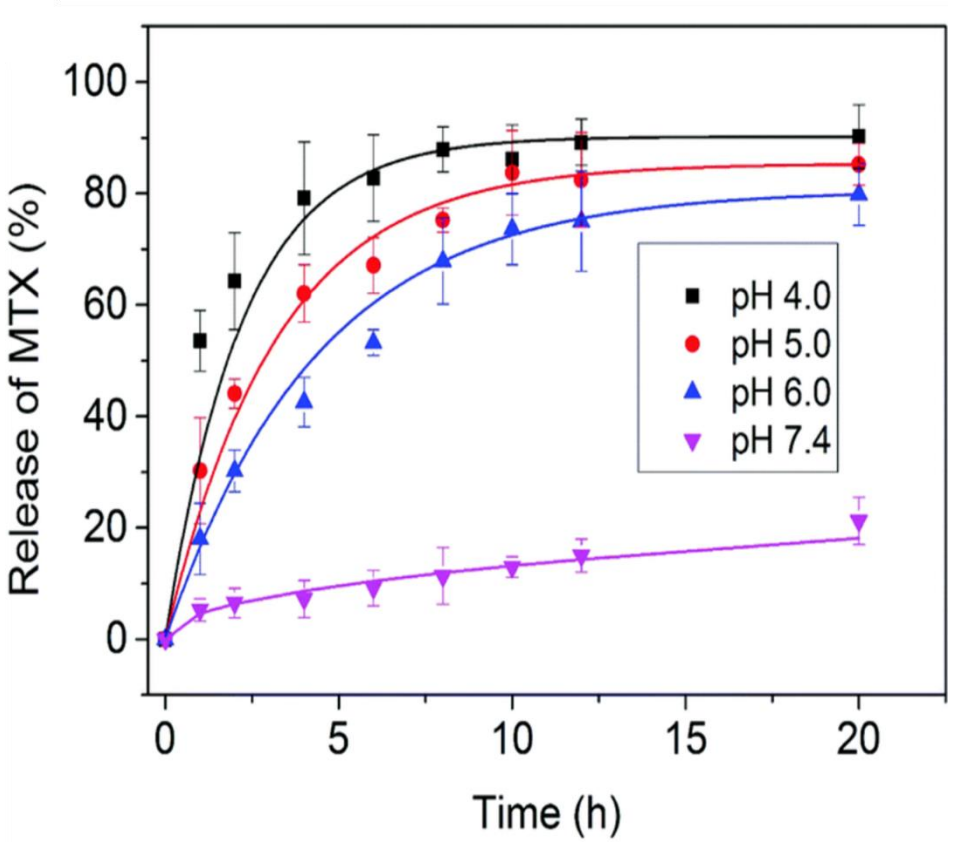

Figure 2.22. Release profile of MTX from MnFe-MTX-LDH in different pH buffers.[43]

Oh et al(2009) evaluated the cellular uptake relative with LDH particles size and they found that the size dependent uptake in osteosarcoma cells in the order of 50 > 200 or = 100 > 350 nm, suggesting that the smaller the particles size is, the easier for LDH particles to penetrating the cellular membranes.[44]

Lately, Li et al (2013) studied the particles size effects on the cellular uptake. They synthesized the Mg_3Al-CO_3-LDH (20 nm) and Mg_3Al-NO_3-LDH (180 nm) and further conjugated with fluorescein isothiocyanate (FTIC) (Figure 2.23). Interestingly they found that those particles with 20 nm, located in the nucleus of Mouse Motor Neuron (NSC 34) cells while the 180 nm LDH nanoparticles located in the cytoplasm.

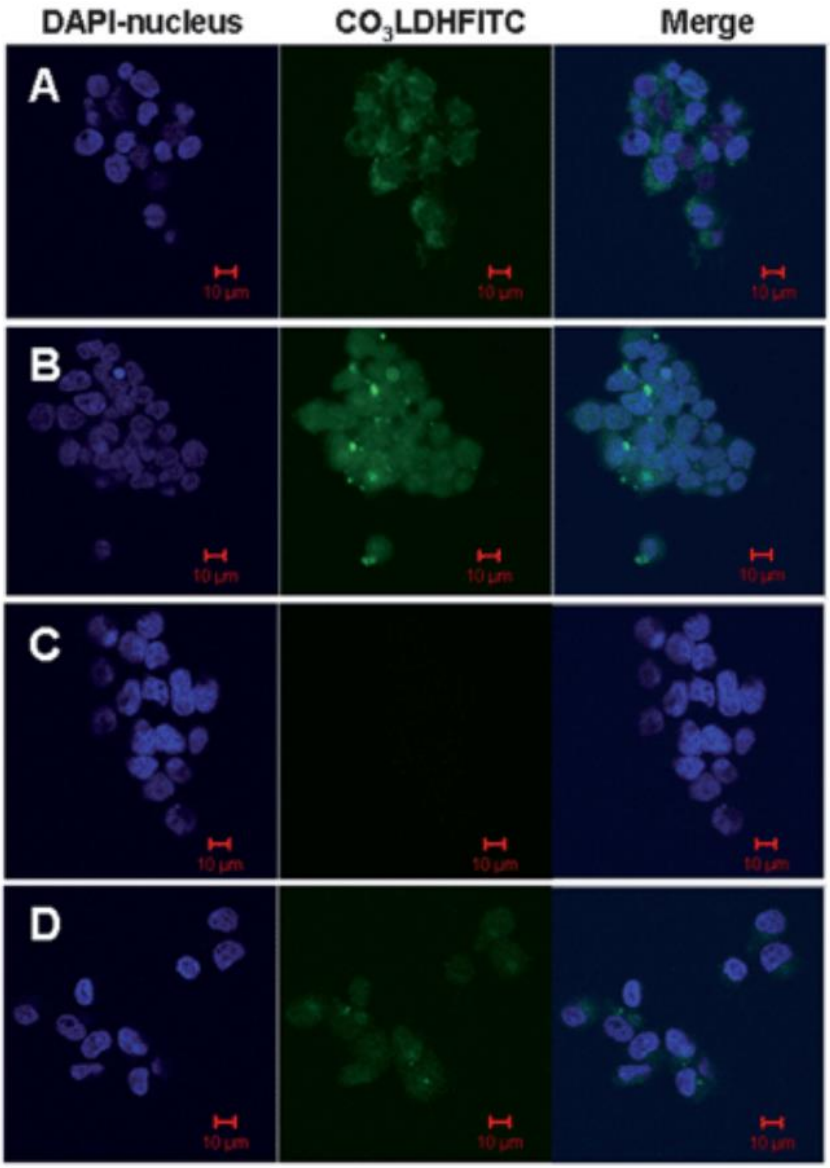

Figure 2.23. Confocal microscopic images of intracellular localization in NSC 34 cells: (A) 6.25 µg ml^{-1} Mg_3Al-CO_3-FITC-LDH, incubated for 2.5 h; (B) 10 µg ml^{-1} Mg_3Al-CO_3-FITC-LDH, incubated for 3 h; (C) control experiment performed with supernatant solution of 17 µg ml^{-1} Mg_3Al-CO_3-FITC-LDH, incubated for 3 h; (D) free 6.25 µg ml^{-1} FITC anions incubated for 4 h [45].

2.6 Nanomotor

Nanomotors, are inspiration based on natural motional behaviors. With the tiny scale, they can accomplish many delicate missions. Unlike the general nanoparticles, under some specific conditions, nanomotors are fully possible to be manipulated. The methods could be light, magnetic field, acoustic, electric field, temperature, pH, chemotaxis and chemicals additives etc.

Dai et al, in 2016 reported a novel type of light sensitive nanomotor.[46] They fabricated a 'tree-like' nanomotor that composed by TiO_2 and Silicon (Figure 2.24). By subjecting a 365 nm ultraviolet, accompany with 0.1% hydrogen peroxide, the nanomotor shows a motional enhancement on the speed, instead of pure Brownian motion. They explained that under the illumination, the photoexcited holes in TiO_2 nanowire and the electrons in the silicon migrate to the semiconductor–electrolyte interface.

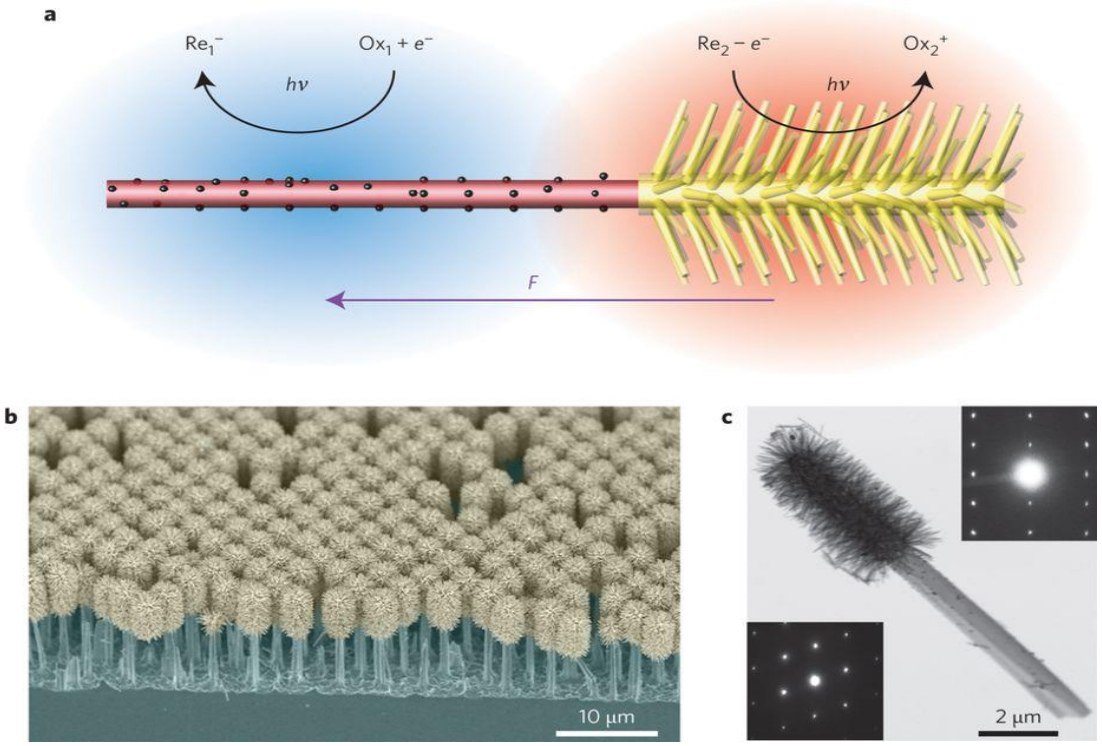

Figure 2.24. a) Schematic of a Janus artificial micro-swimmer an array of TiO_2 nano-tree (yellow) grown on a silicon nanorod(pink) and Platinum (black) nanoparticles, which act as electrocatalyst. b) SEM image of a Janus nano-tree forest prepared on a silicon substrate, colors are re-processed; c), TEM image of one individual Janus nano-tree.[46]

By transferring the electrons within the nanowire, a local electric field can be built up around the charged nano-tree, leading to its autonomous swimming *via* electrophoresis in this self-generated electric field.

Unlike many of the nanomotors, using the hydrogen peroxide as the 'fuel', by decomposing the H_2O_2 and then generating the oxygen as propulsion to propel the nanomotors themselves, the nanowire swimmer motion was streaming from the self- electrophoresis.

The most suitable type of nanomotor for the biomedical use needs to be biocompatible and biodegradable. Therefore, Shao et al and the co-worker, taking the advantages of cells chemotaxis nature, developed a biohybrid micromotors.[47] They constructed the mesoporous silica nanoparticles (MSNs) by camouflaged with *Escherichia coli (E. coli)* membrane, and then use the living neutrophils to engulf the coated MSNs. As expected, the biohybrid micromotors show an obvious directional motion, which toward to the chemoattractant *(E. coli)*. Furthermore, they encapsulated the doxorubicin (DOX) to the EM@MSNs, and the cumulative drug released was significantly suppressed due to the *E. coli* membrane camouflage. In addition, the turning angle distribution (TAD) [48] and chemotactic index (CI) [49] both indicated the biohybrid micromotor has the distinct chemotactic behaviors.

The author took the advantages of neutrophil cells, which are inherent abilities of endocytosis and migration, and achieved a great success of precise-target delivery.

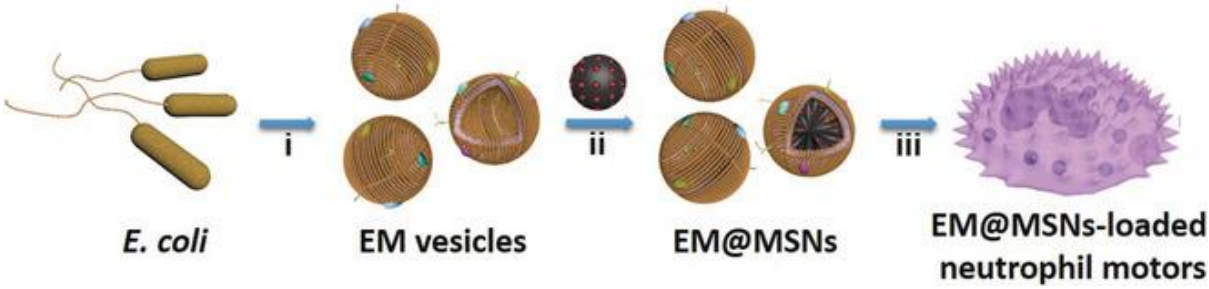

Figure 2.25. Schematic of neutrophil loading *E. coli* membrane coated mesoporous silica nanoparticles.[47]

Gao et al (2019) used Zeolitic Imidazolated Framework-L(ZIF-L) and designed a reversible and pH-stimulated micromotor. By cooperating Zn (II) or Co (II) with imidazolate-type links which is succinated β-lactoglobulin, they also entrap hydrogen peroxide composition enzyme inside the frameworks (Figure 2.26). Together, the nanomotor was capable to block or open pores according to the pH, and therefore allowing hydrogen peroxide access to or away from the enzyme. The enzyme inside the micromotors is capable to decompose the hydrogen peroxide to oxygen. By converting the chemical energy to mechanical energy, the micromotors can therefore propelling themselves. The novel point of this paper is that they manipulate the micromotor autonomous movement *via* pH-control. Specifically, when the micromotors come across the mild acidic pH environment, the succinylated β-lactoglobulin undergo a reversable gelation process, result in preventing the fuel (hydrogen peroxide) access to the enzyme, then the autonomous motion therefore stops. However, if the micromotors are in the neutral pH environment, the hydrogen peroxide can freely access to the enzyme and be decomposed to oxygen.

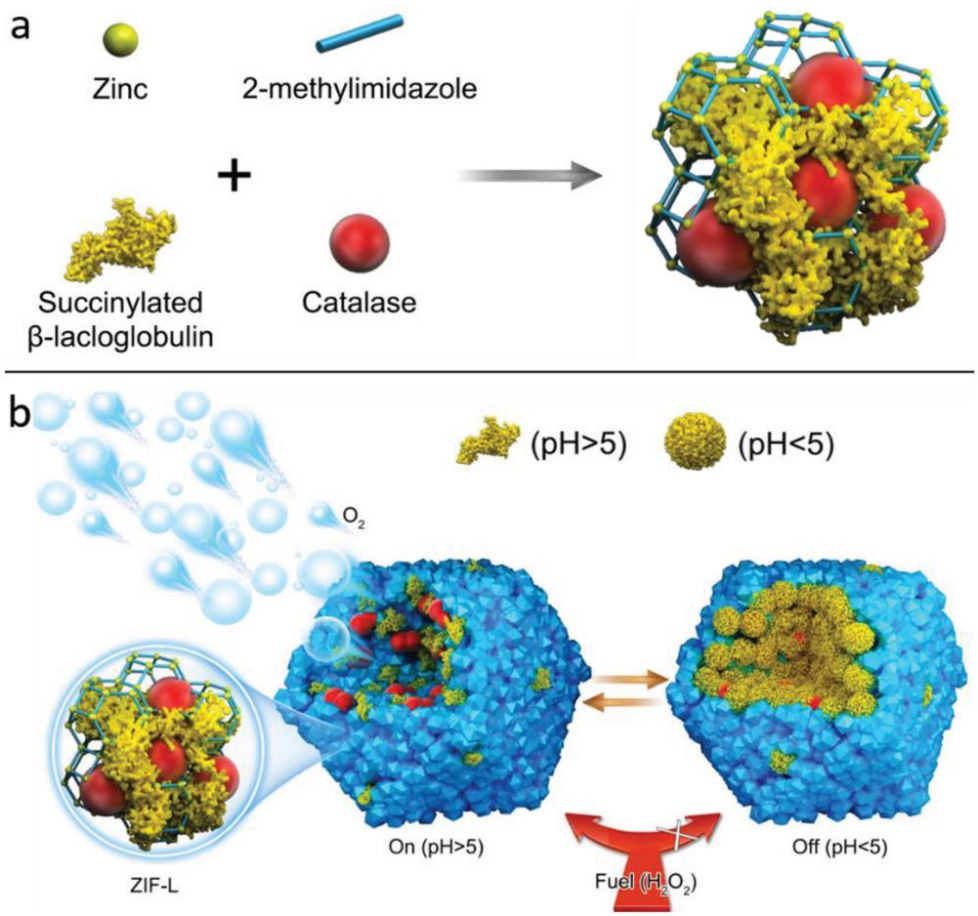

Figure 2.26. Schematic of a) ZIF-8 assembly and b) oxygen generating-phases shifting in different pH.[50]

This material therefore has the great potential of biological implementation due to the fact that the pH in normal organ/tissue is neutral while the inflammation or tumor area has the mild acidic environment. Taking these as advantages, the material is fully capable of fulfilling the drug delivery task.

Guo et al 2019, developed a submarine-like micromotors which can be manipulated the vertical motion *via* controlling pH value.[51] They successfully intercalated bio-enzyme as the catalase in the core, PDPA as the 'wings' (a pH-sensitive polymer) within the metal-organic framework (MOF) particles. With the presence of hydrogen peroxide, the MOF can decompose the

hydrogen peroxide, then the PDPA can interact with the oxygen which generated from the decomposition, depending on the PDPA on phases (pH > 6.4 hydrophobic, pH < 6.4 hydrophilic) to increase the particles buoyancy force and thus control the vertical motion. They further investigated the viability testes on MCF-7 cells and found that the vertical motion preserves within the cells as well as low cytotoxicity.

There are very limited papers that reported regarding the micro/nanomotors that can be manipulated the vertical motions by decomposing the hydrogen peroxide (Figure 2.27).

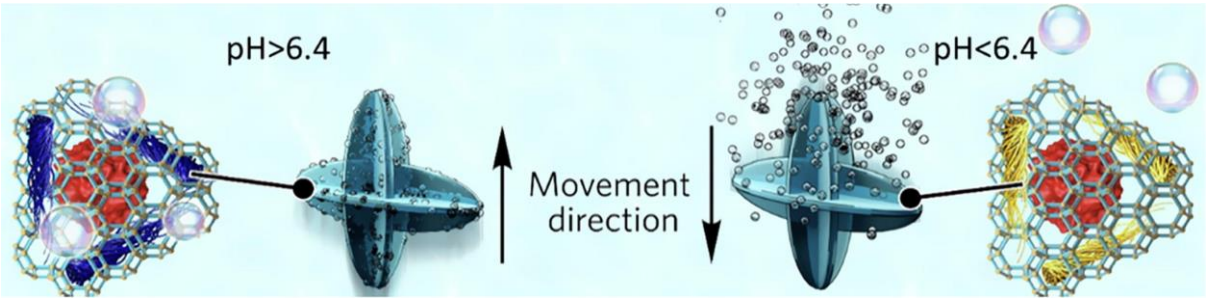

Figure 2.27. Schematic of ZIF-L vertical movement stimulated by pH.[51]

Wang et al (2013) defined the power conversion efficiency of the nanomotor as

$$\eta_{overall} = \frac{mechanical\ power\ output}{total\ chemical\ power\ input} = \frac{P_{mecha}}{P_{chem}}$$

Where $Pmecha$ and $Pchem$ are further defined as

$P_{mecha}=F_{drag}v=fv^2$

$P_{chem}=nO_2 \bullet \Delta_r{}^{\theta}G$

where the f is the frictional coefficient

For sphere nanomotor $f = 6\pi\eta r$, while for cylinder $f = \frac{2\pi\eta L}{\ln\left(\frac{L}{R}\right) - 0.72}$ [52]

Howes et al (2007) investigated the motion behaviors of Pt half-coated Polystyrene microspheres. They pointed out that the motion of the microsphere's motors are the

combination of rotation and the Brownian motion, which lead to the Mean Squared Displacement (MSD) verse time interval not linear but an exponential-like curve.

Therefore, they proposed the expression for $a^2 + b^2 = c^2$

$$\mathrm{MSD} = 4\mathrm{D}\Delta\mathrm{t} + \frac{V^2\tau^2}{2}\left[\frac{2\Delta t}{\tau} + e^{\left(-\frac{2\Delta t}{\tau}\right)} - 1\right]$$

τ is the time of sphere rotation.

for $\Delta\mathrm{t} \ll \tau$, the expression has limiting form of:

$$\mathrm{MSD} = 4\mathrm{D}\Delta\mathrm{t} + V^2\Delta t^2$$

for $\Delta\mathrm{t} \gg \tau$, the expression has limiting form of:

$$\mathrm{MSD} = (4\mathrm{D} + V^2\tau)\Delta\mathrm{t}$$

They then used both two limiting forms of expression to fit the MSD of microsphere, they found that by using $\Delta\mathrm{t} \gg \tau$ form can yield a liner regression line while using the $\Delta\mathrm{t} \ll \tau$ yielded a parabola line. This indicates $\Delta\mathrm{t} \gg \tau$ model fit the microsphere motion behavior, which further indicate the microsphere in low Reynolds number fluid, most of the time that propels in Brownian motion. By combing with Howse et al (2007) models, the velocity of nanomotors can be determined due to the sphere morphology.[53]

Hormigos (2016) and the co-workers attempted the different carbon allotropes nanomaterials, namely 0D (C_{60} fullerene), 1D (carbon nanotubes), 2D (graphene) and 3D (carbon black, CB) assemble with diverse inner catalytic layers (Pt, Pd, Ag, Au, or MnO_2) and test the 'swimming' speed within different mediums (seawater, human serum and juice samples). However, the authors proposed that the reason of causing different speed, is because of the balance between two opposite forces: the increased catalytic activity in the inner catalytic layer and the friction

of the rough out surface with the fluid. A drag force caused by the fluid and a propulsion force caused by the growth and ejection of bubbles. As the speed of micro/nanomotor is relative to the shape, they calculated and find out the carbon-nanotube-Pt (1D) material was the fastest swimmer by using Li's (2015) proposed calculation model.[54]

2.7 Antibacterial treatment

It has been reporting the nano-scale materials show the outstanding performance on antibacterial treatment.[55]

Alimohammadi et al (2018) reported that MnO_2 and MoS_2 nanosheets with blade-like shape that could remarkably killing *B. subtilis* and *E. coli*, rendering the sharp edges of these 2D materials (Figure 2.28).[56].

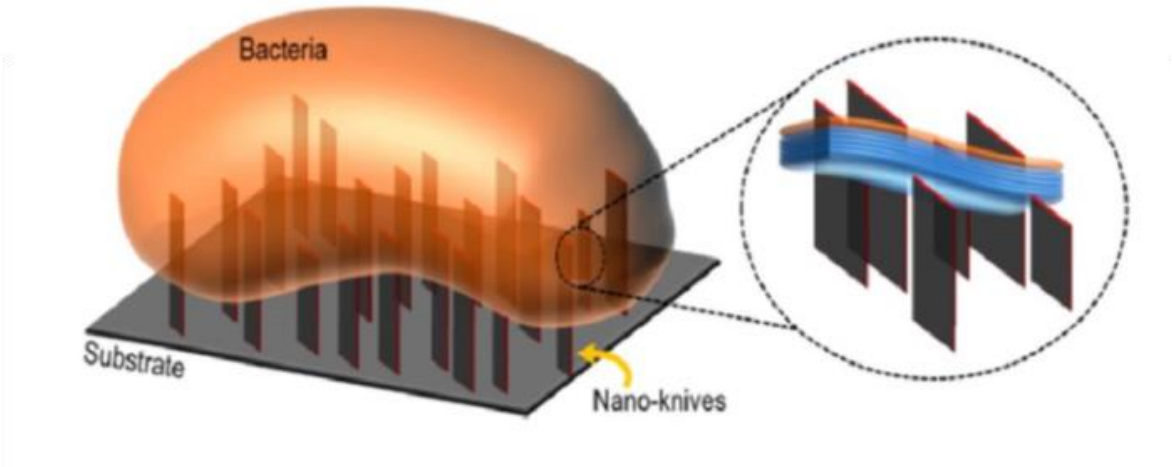

Figure 2.28. Schematic representation of direct physical interaction of the bacterial surface with sharp edges of vertically aligned nanosheets onto a substrate.

Sun et al (2014) reported the graphene quantum dots could catalyze the low concentration hydrogen peroxide decompose and selectively generate the reactive oxygen species generation (Figure 2.29). According to their antibacterial experiment results, the growth of both gram-positive and gram-negative types of bacterial were significantly inhibited rendering the radicals interrupting the bacterial membranes formation.[57]

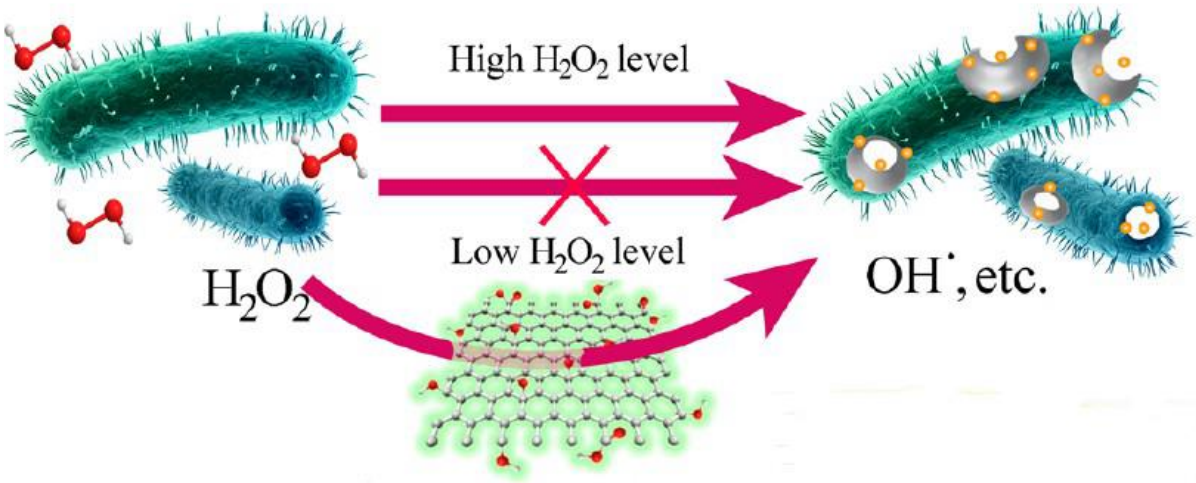

Figure 2.29. Schematic illustration graphene quantum dots catalyzing reactive oxygen species radical generation and therefore killing microbes.

Recently, Xu et al (2018) proposed a novel nano-conversion strategy for enhancing antibacterial activity (Figure 2.30). By converting natural organosulfur compounds into nano-iron sulfides (FeS), the enhanced antibacterial effect was attributed to cysteine-nFeS (Cys-nFeS) with enzyme-like activity could effectively increase the release of bactericidal polysulfides.[58]

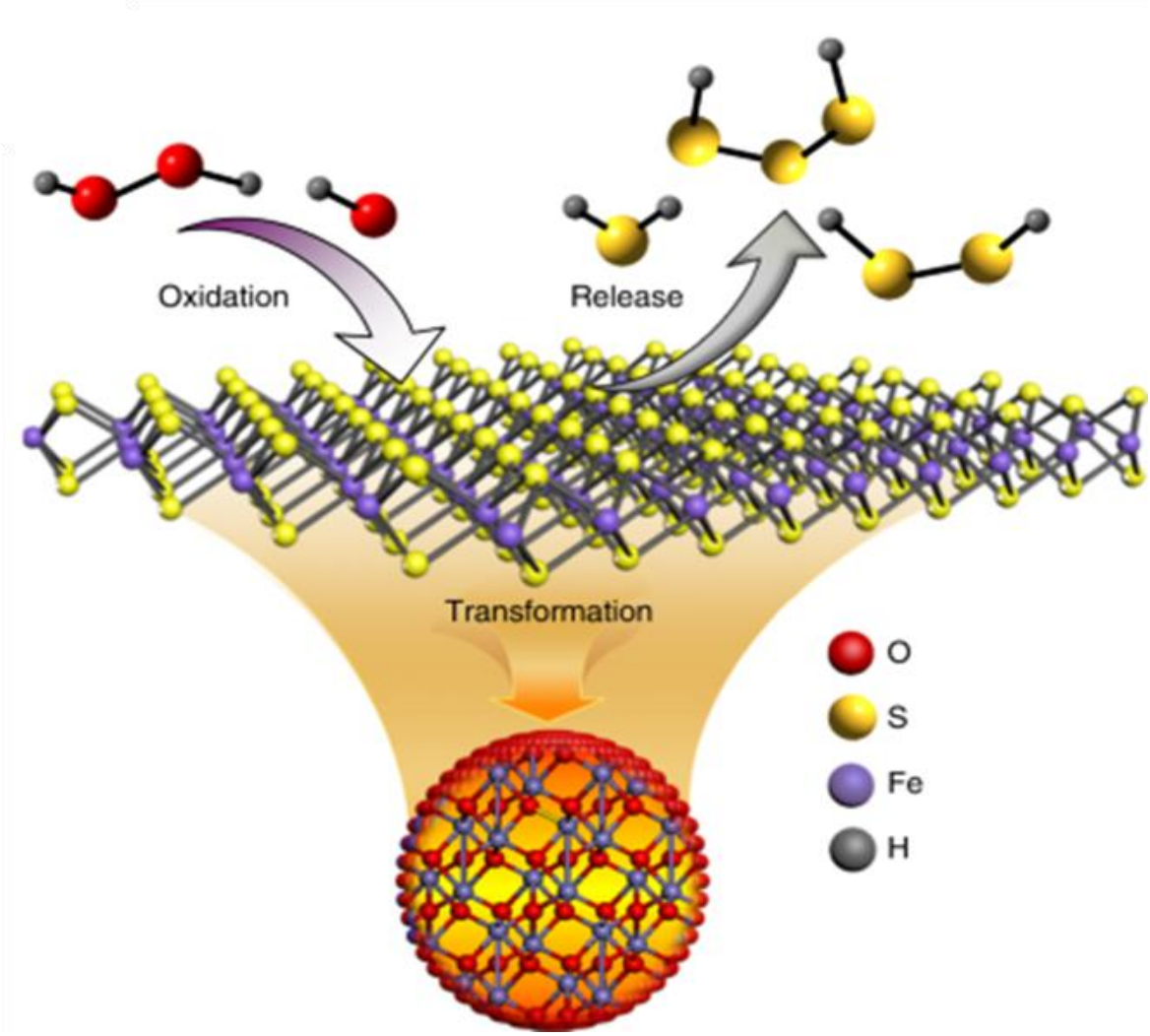

Figure 2.30. Scheme of polysulfane release from nFeS

Chapter 3
Ferrous Ions Containing Layered Double Hydroxides (LDHs) Nanomotor for Tumor Therapy

3.1 Introduction

Inspired by the thrusting mechanism in nature, synthetic micro- and nano-scaled motors have been constructed as an intelligent and multifunctional platform with potency to revolutionize biomedical technology.[59-62] Chemically-driven micro/nanomotors are of interest in many applications because this type of motors are able to selectively react with unique chemical components in the local biological environment and convert the chemical energy to mechanical energies that enable propulsion of the micro/nanomotors, thus achieving stimuli-responsiveness without an external energy input.[63, 64] For instance, biocatalytic metal-organic framework particles were developed as pH and H_2O_2 dual-responsive micromotor that can potentially fulfil tumor-targeted drug delivery.[50, 51] Magnesium microparticles were designed to respond to the gastric acid environment for oral anti-virulence vaccines[65] and cargo protection.[66]

Compared to the micromotors, nano-scaled motors are generally favorable for in vivo practical applications, given that they are more likely to penetrate in deep tissues and be readily internalized by living cells. However, due to the strong Brownian motion and low Reynolds numbers induced by the small scale, the nanoparticle movement regulation is still challenging for real implementation.[67-69] To overcome random diffusion and achieve directional motion in biological environment, the incorporation of endogenous enzymes (e.g. catalase, glucose oxidase) in the nanomotor system has been adopted as a strategy to produce propellent.[70-72] However, this strategy may pose additional complexity in terms of synthesis and scaling as well as uncertainty of the system.

Two-dimensional (2D) nanomaterials have demonstrated significant potential in energy-

related and biomedical applications with excellent performance in catalysis and drug delivery.[73, 74] Specifically, the large specific surface area of 2D nanomaterials provides a large amount of catalytic sites and anchoring points, which enables high levels of catalytic activities and cargo-loading capacity.[75] Layered double hydroxide (LDH) is a group of typical 2D nanomaterials with many unique merits such as tunable physiochemical structure, desired biosafety and biodegradable ability.[4, 35] The traditional LDH is featured by a multilayered structure and consists of brucite-like layers and interlayer anions.[1] Notably, even higher surface area can be achieved by constructing monolayer LDH nanosheets.[22] Recently we have developed a facile, effective and low-toxic method to produce monolayer and well-dispersed LDH nanosheets that demonstrated the excellent peroxidase-like activity to catalyze H_2O_2 to produce reactive oxygen radicals.[35] The LDH nanosheets also displayed pH-responsive biodegradability that guaranteed their biosafety for practical in vivo applications. The findings inspired us to further explore the catalase-like activity of the LDH nanosheets, which could help fill the gap of smart nanomaterial design and realize the full potential of nanomotors.

Herein, we reported a catalase-like, LDH nanosheet-based 2D nanomotor that is able to deliver cargo and directionally move toward the tumor microenvironment. To enable high degree of chemical-to-mechanical energy conversion, we incorporated ferrite and ferrous ions in a 2D monolayer metal hydroxide nanosheet. Polyethylene glycol (PEG) was used as a layer growth inhibitor to construct monolayer LDH nanosheet and also helped maintain colloidal stability of the nanosheets in biological solutions, and thus exposed maximal catalytic sites for high catalytic efficiency in practical bio-applications. We found the nanosheet generated oxygen bubbles and promoted the long travel distance only with presence of both hydrogen

peroxide (H_2O_2) and slightly acidic/neutral pH (key characteristics in the tumor microenvironment). Very interestingly, this tumor microenvironment-responsive movement has chemotactic properties, which was evidenced by the directional movement of the nanosheet toward higher H_2O_2 environment. Using doxorubicin as a model drug, we confirmed the feasibility of using the 2D nanomotor for efficient drug delivery to breast cancer MCF-7 cells. By virtue of its nanoscale size, stimuli-responsive catalase-like performance, chemotaxis-guided movement properties, and biodegradability, we envision that this 2D nanosheet may serve as an advanced nanoplatform for a broad scope of biomedical applications.

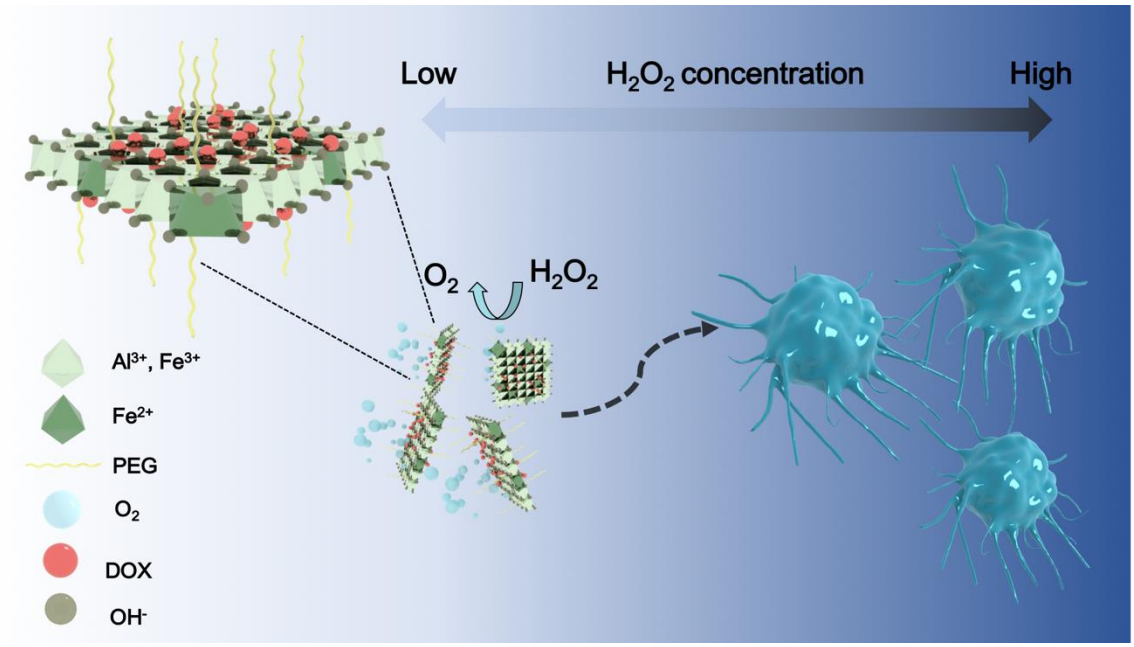

Figure 3.1. Schematic illustration of the 2D LDH nanomotor and its directional movement toward the tumor microenvironment.

3.2 Experimental Section

Synthesis of Nanoparticles: The PEG/Fe-LDH nanoparticles was prepared *via* co-precipitation with addition of dual phosphonic acid-polyethylene glycol diblock copolymer (PEG) (molecular weight = 10 000 g mol^{-1}, degree of polymerization = 22) [35]. Briefly, the

$FeCl_2$ (0.2536 g, 2 mmol) and $AlCl_3 \cdot 6H_2O$ (0.2414 g, 1 mmol) was dissolved in degassed Milli-Q, and then, mix with 6 mmol of NaOH with constant pH under nitrogen atmosphere. Next, the 0.2 g PEG (molecular weight ≈ 10000)) was added into the mixture (Fe-LDH synthesis has skipped this step), followed by hydrothermally treatment at 100 °C for 8h. The LDH particles were obtained after 3-times centrifugation. Similarly, the PEG/Mg-LDH was prepared by using the similar procedure but substituting $FeCl_2$ to $MgCl_2 \cdot 6H_2O$.

Loading DOX and FITC: 100 μL of freshly prepared PEG/Fe-LDH was diluted to 5 mL and degassed. After that, the diluted LDH was pre-heated to 37 °C with nitrogen protection, and then 5 mL of DOX solution was added into the LDH under vigorous string after adjusting the pH to 8.0 by NaOH (DOX: LDH mass ratio of 1.25:1). After reacting for 2 h, the mixture was centrifuged one time to remove un-saturated DOX. The encapsulation efficiency (71.31%) and loading capacity (89.14%) were calculated by comparting the DOX concentration in the supernatant after loading against a predetermined calibration curve. The DOX@PEG/Mg-LDH and FITC@PEG/Fe-LDH were prepared *via* the similar procedure but replace the PEG/Fe-LDH to PEG/Mg-LDH or replace the DOX to FITC.

NanoSight Procedure: LM10 module of NanoSight was used to record the particles movement coordinates. 1 mL of 0.2 M HAc-NaAc buffer was mixed with 2 μL of PEG/Fe-LDH (4.8 mg mL^{-1}). After that, 10 μL of H_2O_2 (0.3% and 3% w/w) was added into the mixture, and then the solution was put onto vortex mixer to mix before injecting the solution into the chamber. The *x y* coordinates were plotted into ImageJ to reproduce the particles trajectories and to calculate the *MSD* and diffusion coefficient.

Chemotactic Behaviors: The chamber was filled with 2 mL of water with addition of

different reagents and then observed under the fluorescence microscope (Olympus IX 53 module) with x60 oil-immerse objective lens. After that, 20 μL of hydrogen peroxide (0.3% and 3% w/w) was gently added to one round orifice before 4 μL of DOX-loaded LDH was added into the opposite orifice. The fluorescence images were obtained by using TRTIC filter and the consecutive images were acquired in 25 ms time interval.

Cytotoxicity Assay: MCF-7 cells were seeded in 96-well microplates (1×10^4 cells in 100 μL DMEM) and allowed to adhere overnight. The cell culture medium at pH 7 was used to simulate the extracellular microenvironment in a solid tumor. Hydrochloric acid was added to the DMEM in order to neutralize to a pH of 7. The culture medium was then replaced with fresh DMEM (pH 7) containing DOX@PEG/Fe-LDH particle (corresponding DOX concentrations of 0.2, 0.5, 1, 2, 5 and 10 μg mL^{-1}). After 24 hours incubation, cell viability was determined by CCK-8 assay and the absorbance of samples was measured on a microplate reader. The experiments were carried out in triplicate.

Cellular Uptake: MCF-7 cells were seeded in a 24-well plate with coverslips at a density of 5×10^4 cells per well. At around 50% confluency, culture medium was replaced with medium containing FITC@PEG/Fe-LDH (10 μg mL^{-1}). After a pre-determined incubation time (4 h and 24 h), cells were washed with PBS three times. After that, the lysotracker deep red (50 nM) was added and incubated 1h, followed by washing with PBS three times. Next, cells were fixed with 4% PFA, and the coverslip mounted on glass slides with ProLong® Gold Antifade Mountant with DAPI. The cellular uptake of FITC@PEG/Fe-LDH were observed under Olympus IX53 fluorescent microscope.

Biodegradation assay: The PEG/Fe-LDH nanosheets were suspended in the 0.2 M of

HAc-NaAc buffer of pH 5.0 and pH 7.0. After 2 h incubation, an aliquot (100 μL) was collected to prepare TEM samples, and the particle morphology was observed under the JEOL 1400 transmission electron microscope.

3.3 Results and Discussion

3.3.1 Physicochemical properties of nanomotor

The 2D catalase-like nanomotor (PEG/Fe-LDH) was synthesized by co-precipitating alkaline and catalyst metal ions (Fe(II) and Fe(III)) followed by hydrothermal aging.[35] To expose maximal catalytic sites and boost catalytic efficiency, 2D monolayer nanosheet with high surface density of active catalytic metal ions was designed and synthesized by introducing PEG during the synthetic procedure as a layer growth inhibitor and stabilizer. Transmission electron microscopy (TEM) image reveals that the PEG/Fe-LDH has the suborbicular shape with the lateral diameter around 100 nm (Figure 3.2a).[41] The nanosheet thickness was measured to be around 2.5 nm by atomic force microscopy (AFM), which is in accordance with the monolayer LDH nanosheet topology (one sheet of brucite-like layer and PEG on the surface) (Figure 3.2b).[35] From the X-ray diffraction patterns, the characteristic peaks (00l) with the diffraction peaks of (003) at $2\theta = 11.69^{o}$ and (006) at $2\theta = 22.59^{o}$ that were shown in pristine Fe-LDH nanoparticles could be hardly identified in the PEG/Fe-LDH (Figure 3.2c). This indicates the lack of long-range ordered structure in the PEG/Fe-LDH and the successful formation of monolayer nanosheets.[76] From the Fourier-transform infrared spectroscopy spectrum, stretching vibration of C-O and C-H alkyl group from PEG molecules was recorded at 1104 cm^{-1} and 2920 cm^{-1} respectively in the PEG/Fe-LDH spectrum, which was not

observed in the Fe-LDH spectrum, suggesting the attachment of PEG on the PEG/Fe-LDH nanosheet (Figure 3.2d).[36, 77] The weight ratio of PEG in the nanosheet was quantified to be 5.69% (Figure 3.2e). PEG acts not only as a layer growth inhibitor, but also as colloidal stabilizer that prevented nanosheet aggregation in electrolyte solutions, which was evidenced by the similar hydrodynamic sizes (~200 nm) of the PEG/Fe-LDH in water and different buffer solutions (cell culture medium, saline and PBS) (Figure 3.2f). The improved colloidal stability facilitated by the surface PEG helps expose maximal catalytic sites to reactants, and thus could be beneficial to realize high level of catalytic performance.

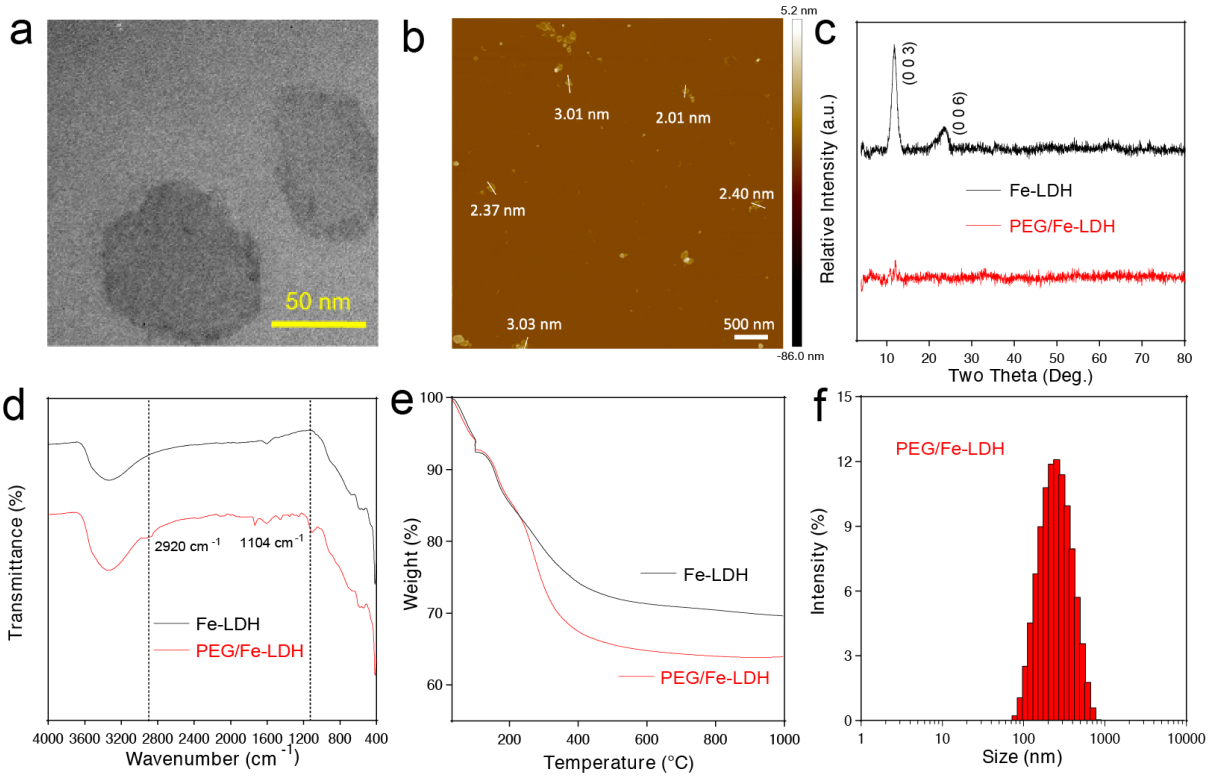

Figure 3.2. Physicochemical properties of the PEG/Fe-LDH and Fe-LDH nanomotors. a) TEM image, b) AFM image, c) XRD patterns, d) FTIR spectra, and e) TGA curves of PEG/Fe-LDH compared to those of Fe-LDH particles and f) hydrodynamic size distribution of PEG/Fe-LDH particles.

3.3.2 Stimuli-responsive motion behavior

The stimuli-responsive movement of PEG/Fe-LDH nanomotors was investigated by measuring the travel distance of the nanomotors in buffer solutions with different concentration of H_2O_2 and pH values. Specifically, the nanoparticle-tracking analysis (NTA) was used to record the *x* and *y* coordinates of the real-time movement of individual nanomotors and provided individual particle-by-particle analysis. These data were further used to calculate the average mean square displacement (*MSD*, a typical metric for quantifying particles' migration speed and distance traveled) curves of particles by using the equation $MSD = (x_t - x_0)^2 + (y_t - y_0)^2$.[78] When H_2O_2 was absence in the buffer solution, the particles showed typical random-walk at both pH 5 and pH 7. With addition of H_2O_2 (final concentration of 0.03% w/w) the travel distance of nanomotors was obviously longer at pH 7 than that at pH 5 and the group without H_2O_2, showing the dual stimuli-responsive motion of the PEG/Fe-LDH nanomotor (Figure 3.3a). This phenomenon corresponds to the pH-responsive O_2 generation ability of the PEG/Fe-LDH. In the buffer solution at pH 7 with addition of PEG/Fe-LDH, a large amount of oxygen generated (Figure 3.3d and 3.3e) and serve as the propellant to promote the motion of the PEG/Fe-LDH nanomotor. Also, the PEG/Fe-LDH nanomotor showed fuel concentration-dependent motion behavior. As the fuel (H_2O_2) concentration increased from 0.003% to 0.03%, the nanomotor could rapidly convert the chemical energy to mechanical power to propel themselves and move faster.

To gain further understanding of the stimulation effects, the diffusion coefficient (D) was introduced to relate the *MSD* with the time. As the *MSD* grows linearly with time, the diffusion coefficient can be calculated by using the formula $D = MSD / (i \times \Delta t)$,[78] where *i* is the

dimensional index; In the two-dimension cases, i equals to 4;[79] t is the time interval. In this way, the movement enhancement in different conditions can be indicated distinctly. The diffusion coefficient of the PEG/Fe-LDH at pH 5 with the final concentration of 0, 0.003% and 0.03% (w/w) H_2O_2, was calculated to 0.87, 0.91 and 1.11 $\mu m^2 s^{-1}$ respectively (Figure 3.3c). It is worth noting that at pH 7, the diffusion coefficient of the nanomotors significantly increased to 1.05, 1.69, and 3.07 $\mu m^2 s^{-1}$ in presence of 0, 0.003% and 0.03% (w/w) H_2O_2. Under chemical power (pH 7, with 0.03% w/w H_2O_2), the diffusion coefficient of the nanomotors could enhance up to 292% compared to their Brownian motion counterpart.

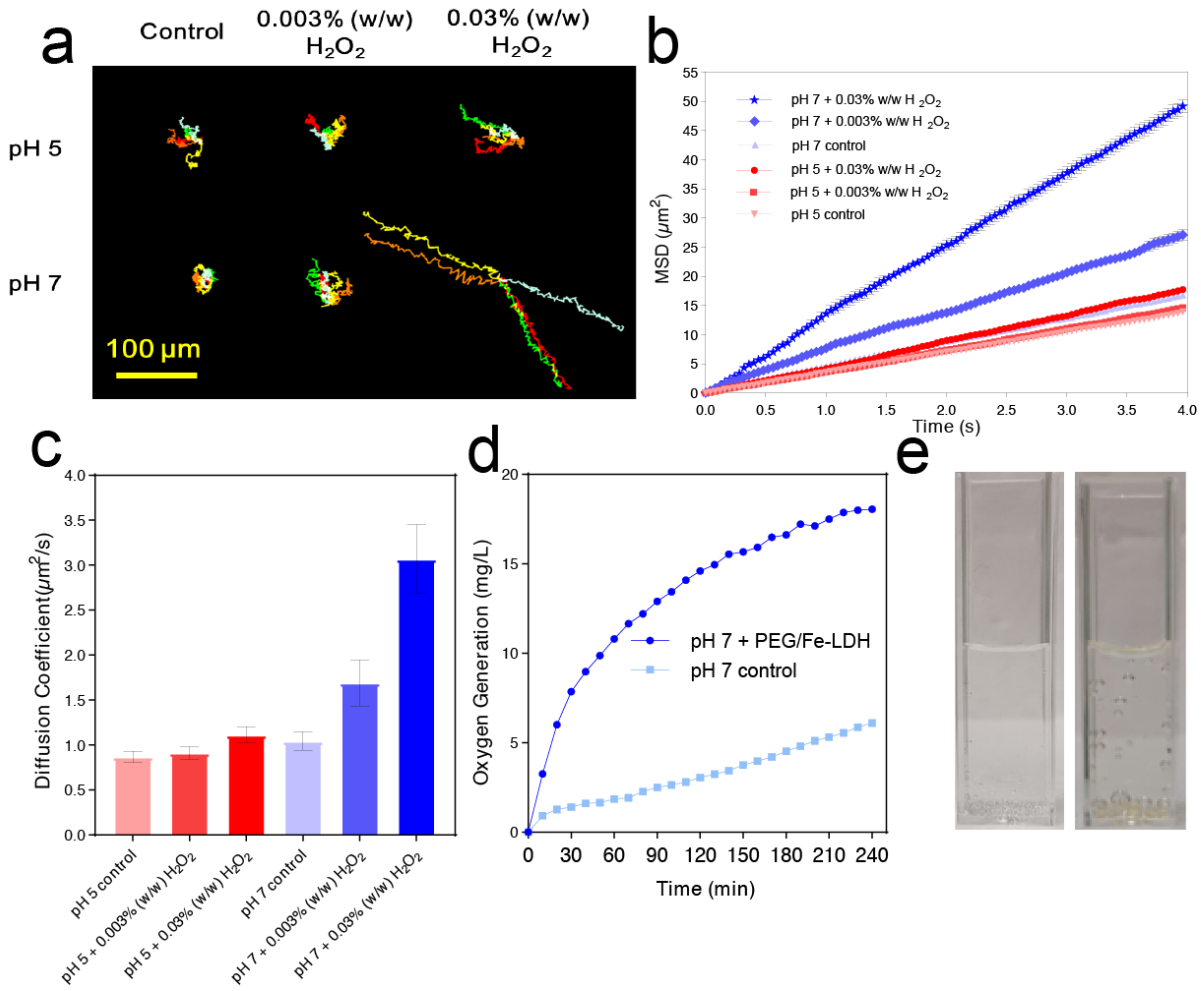

Figure 3.3. Stimuli-responsive movement and O_2 generation of PEG/Fe-LDH nanomotors. a) Trajectory tracking of 5 particles for 4 seconds at different pH values and various

concentrations of H_2O_2. b) *MSD* plot versus time interval, analyzed from *x* and *y* coordinate tracking of at least 20 particles at each condition. c) Diffusion coefficient values calculated from *MSD*. d) Oxygen generation in the pH 7 buffer solution containing 0.3% (w/w) H_2O_2 with or without addition of PEG/Fe-LDH and e) the corresponding images (left: pH 7 control; right: pH 7 with PEG/Fe-LDH under 0.3% (w/w) H_2O_2).

3.3.3 Chemotactic behaviors evaluation

To evaluate the chemotactic behavior of the 2D nanomotors, the PEG/Fe-LDH particles were loaded with fluorescent anticancer drug doxorubicin (DOX) and observed in a homemade 'cassette-like' flow channel under a fluorescence microscope (Figure 3.4a). The particles were added at Point A, while chemoattractant H_2O_2 was originally located at Point B (Figure 3.4a). Under the fluorescence microscope, the directional movement of PEG/Fe-LDH particles toward H_2O_2 was clearly observed (Figure 3.4c). As the concentration of H_2O_2 increased from 0.003% to 0.03% (w/w), the faster movement of the PEG/Fe-LDH was observed. To gain insight into the differences, the x and y coordinates were tracked under the optical microscope and the diffusion coefficient was calculated by using $D = MSD / (i \times \Delta t)$ described previously. For the DOX@PEG/Fe-LDH only without addition of H_2O_2, the mean diffusion coefficient was calculated to 0.83 $\mu m^2\ s^{-1}$ (Figure 3.4b), which was consistent with the results obtained from the pure Brownian motion (Figure 3.3c), indicating the typical 'random walk' of the DOX@PEG/Fe-LDH particles. Similarly, DOX@PEG/Mg-LDH nanoparticles that contains Mg (II) instead of Fe (II) and Fe (III) were not capable of catalyzing O_2 generation from H_2O_2, and in turn only showed the Brownian motion even in the presence of H_2O_2 (D = 0.79 $\mu m^2\ s^{-1}$). In contrast, for the group of DOX@PEG/Fe-LDH with H_2O_2 (0.003% and 0.03%), the

diffusion coefficient increased to 1.08 and 2.09 $\mu m^2 s^{-1}$ respectively, indicating an external power being generated in the presence of the nanomotor and H_2O_2. Apparently, these diffusion coefficient values (1.08 and 2.09 $\mu m^2 s^{-1}$) were smaller than the counterparts obtained from the previous motion study (1.69 and 3.07 $\mu m^2 s^{-1}$ observed from the NanoSight). This is likely due to the lower concentration of H_2O_2 at the site closer to Point A in the chemotactic study. The chemotactic behaviors of the PEG/Fe-LDH particles can be explained by the fact that, the particle motion at higher concentration of the fuel H_2O_2 is faster than that at lower concentration of H_2O_2, leading to the movement toward the higher fuel gradient (chemoattractant).[80]

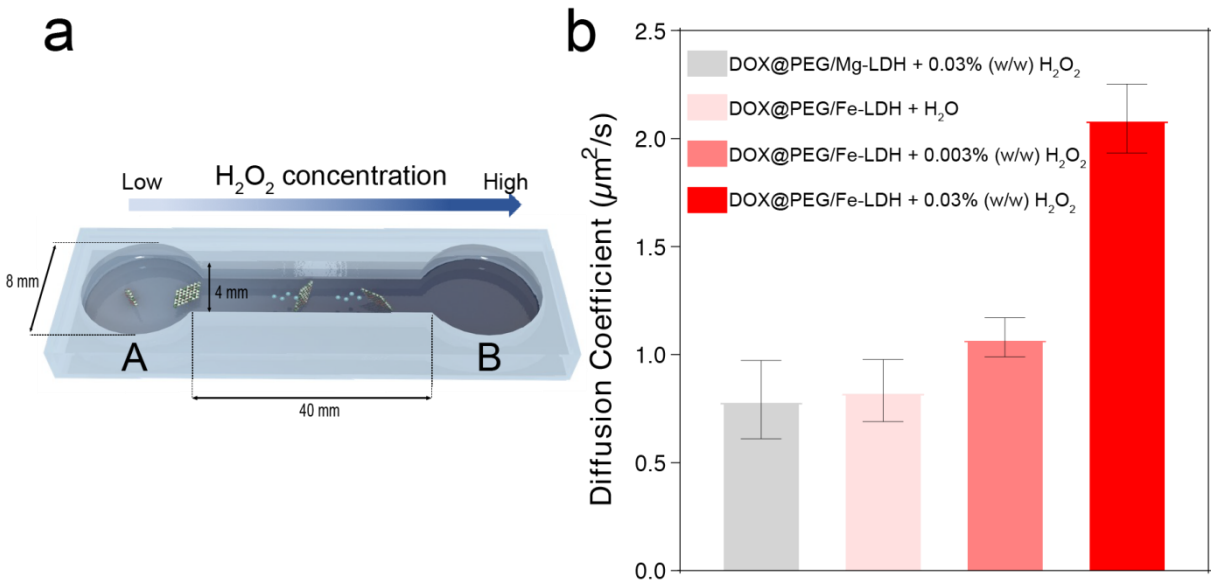

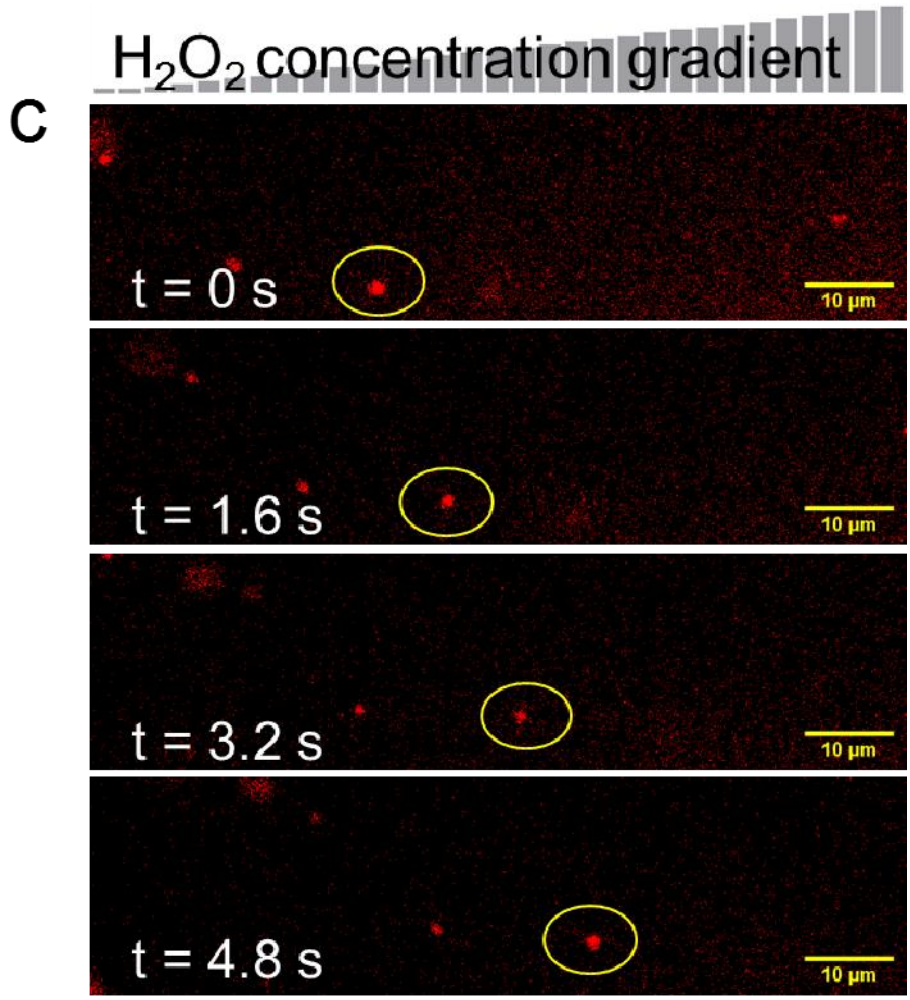

Figure 3.4. Chemotaxis evaluation of DOX@PEG/Fe-LDH nanomotors. a) Micro channel design. b) Diffusion coefficient of DOX@PEG/Mg-LDH and DOX@PEG/Fe-LDH in presence of different concentrations of H_2O_2. c) Time-dependent trajectories of DOX@PEG/Fe-LDH with the addition of 0.03% (w/w) H_2O_2.

3.3.4 Cellular behaviors

Given that the characteristic properties of the tumor microenvironment (overexpressed H_2O_2, mild acidity and hypoxia) provide the favorable conditions for O_2 generation and directional motion of our nanomotor,[81] the catalase-like PEG/Fe-LDH nanomotor holds great promise to be widely adopted in the biomedical field to address key issues in drug delivery, O_2-

dependent therapeutic and diagnostic approaches. To assess the potential application of the PEG/Fe-LDH nanomotor, DOX was adopted as a model drug to be incorporated in the PEG/Fe-LDH particles for drug delivery evaluation (encapsulation efficiency (71.31%) and loading capacity (89.14%)). Breast cancer cells (MCF-7) were cultured in pH 7 growth medium containing 100 μM H_2O_2 to mimic the tumor microenvironment. After 24 h treatment with different concentrations of DOX@PEG/Fe-LDH, cell viability assessment revealed a dosage-dependent inhibition on cell growth with IC50 being 1.559 μM (Figure 3.5b). This cellular suppression behavior can be accredited to associated drug release profile and cellular transport performance. Firstly, from the drug release experiment, we found that the drug release of DOX@PEG/Fe-LDH was significantly faster in presence of higher concentration of H_2O_2. For example, at 4 h, there was 7.67 ± 1.23 % of loaded DOX released from the nanomotor in the medium of 0.03% H_2O_2, compared to 3.37 ± 0.14 % of DOX released in the medium of 0.003% H_2O_2. The assumption that can explain this phenomenon is that when the nanoparticles diffuse faster, the loaded DOX exchanged with the ions in the solution and diffused from LDH surface to the release medium solution at a higher release rate. It is worth to note that solutions in the cell culture and drug release experiments contain homogenously dispersed H_2O_2, while in vivo tumor tissues with presence of H_2O_2 concentration gradient could trigger chemotaxis-driven motion of nanoparticles and enable higher drug release rate and increased cell death. Secondly, DOX@PEG/Fe-LDH exhibited 'endosomal escape' behavior that helped preserve the therapeutic function of loaded DOX prior to reaching nuclei where it exerts function.[82, 83] The fluorescence images of the DOX@PEG/Fe-LDH-treated cells exhibited a large amount of co-localization of endosomes and DOX after 4 h incubation, indicating the internalization of DOX

in the endosomal compartments which showed a typical endocytosis pathway (Figure 3.5c).[84] After 24 h incubation DOX@PEG/Fe-LDH were subsequently released from the endosomes/lysosomes and located in cytoplasm (Figure 3.5d). Next, endosomal escape-associated particle biodegradability was evaluated under TEM after suspending the particles in buffer solutions of pH 5 and pH 7 (to mimic lysosomal acidity and the tumor microenvironment pH respectively) for 2 h (Figure 3.5e). In the pH 5 buffer, no typical LDH shape could be observed, indicating the collapse and disintegration of LDH nanosheets under lysosomal acidity (Figure 3.5f). The acidity-triggered nanosheet degradation not only could lead to endosomal escape observed in the fluorescent images but also could be attributed to biosafety as a drug carrier. Meanwhile, in the pH 7 buffer solution, the LDH structure remained intact without degradation, which could be beneficial for the LDH nanomotor serving as a chemotaxis-driven nanomotor in the tumor environment.

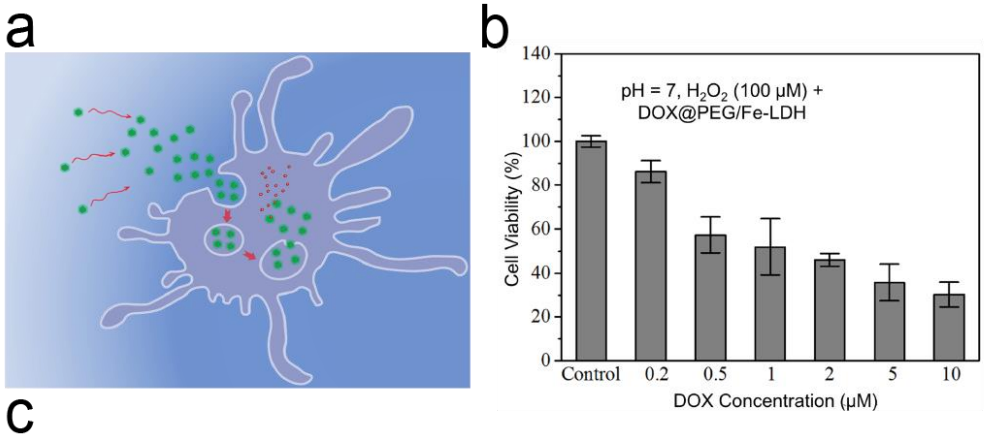
a
b
pH = 7, H_2O_2 (100 μM) +
DOX@PEG/Fe-LDH
Cell Viability (%)
140
120
100
80
60
40
20
0
Control
0.2
0.5
1
2
5
10
DOX Concentration (μM)

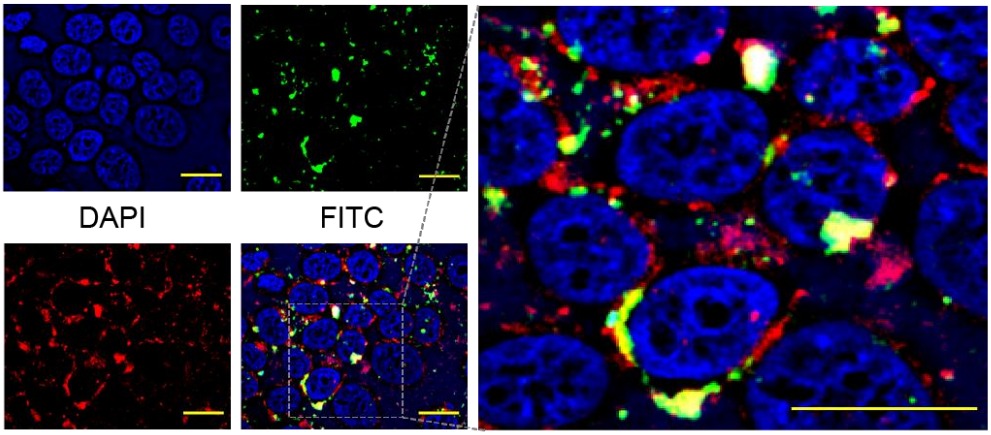
c
DAPI
FITC
Lysotracker
Merged

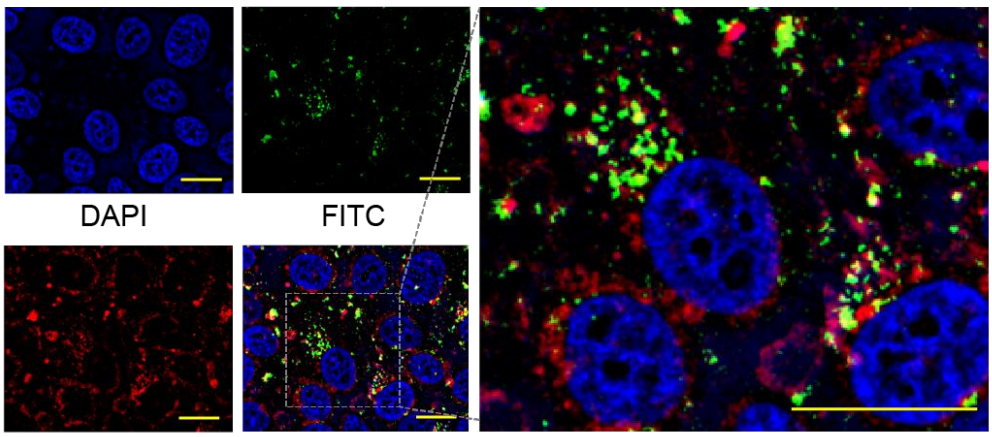
d
DAPI
FITC
Lysotracker
Merged

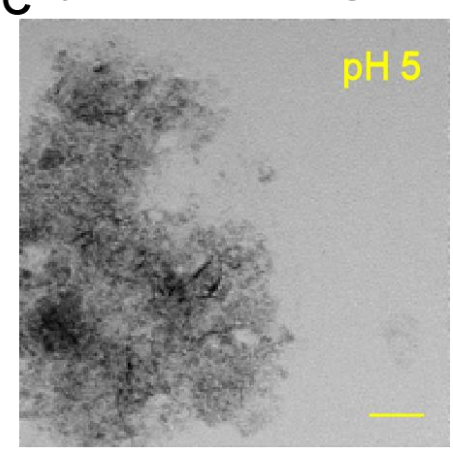
e
pH 5

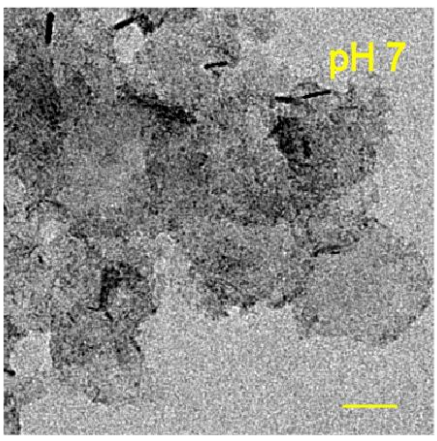
f
pH 7

Figure 3.5. Cellular studies of PEG/Fe-LDH particles. a) Schematic illustration of cellular uptakes of FITC@PEG/Fe-LDH followed by the release of particles from lysosomes/endosomes. b) MCF-7 cell viability after 24-hour incubation with different concentrations of DOX@PEG/Fe-LDH particles. Fluorescence microscope images of MCF-7 cells treated with DOX@PEG/Fe-LDH for c) 4 h and d) 24 h (Blue: DAPI; Red: Lysotracker; Green: FITC@PEG/Fe-LDH; scale bar: 20 μm). Biodegradation performance of PEG/Fe-LDH in buffer of e) pH 5.0 and f) pH 7.0 for 2 h (scale bar = 50 nm).

3.4 Conclusion

In conclusion, 2D catalase-like nanomotors with tumor microenvironment-triggerable movement performance were developed. The 2D iron-containing nanomotor particles were constructed *via* a facile co-precipitation method with introducing of PEG that enables the formation of ultrathin nanosheet particles. In slightly acidic/neutral solutions, the 2D nanomotor could efficiently catalyze H_2O_2 into O_2 and propel the motor particles and exhibited stimuli-responsive movement. The nanomotor could not only travel longer distance in presence of stimuli (H_2O_2 and pH 7) but also swim directionally toward the high gradient of the fuel H_2O_2. The cellular studies of DOX-loaded nanomotors were conducted to further demonstrate the potential drug delivery application of the nanomotors. The DOX-loaded nanomotor particles could efficiently inhibit MCF-7 cancer cell growth at a low dosage, which could be associated with the movement-enhanced drug release behavior and endosomal escape mediated drug transport performance. The pH-responsive biodegradable ability of the nanomotor could be attributed to their dual functionalities as both nanomotor and drug carrier. The

abovementioned catalytic activity, chemotactic movement, biodegradability, and cellular performance enable the 2D nanomotor to be a potent intelligent vehicle for controlled drug delivery, which can function as a standalone drug carrier or alternatively a component in a smart drug delivery system.

Chapter 4
Ferrous Ions Containing Layered Double Hydroxides (LDHs) Nanohybrid for Antibacterial Treatment

4.1 Introduction

Microbes can be problematic due to the fact that the microbe could lead to objects, food and water contamination, moreover, they could cause infection or inflammation in all life forms. The conventional ways to fight against the microbes mainly *via* using the disinfectants or taking antibiotic drugs. Some of them may eliminated the microorganism in a short time, but there were reports that the microbe could adapt the treatment and adjust itself *via* variation, leading to the treatment losing effectiveness and the bacteria was harder to be killed. Meanwhile, the antibiotic drugs could sometimes cause severe side effects to the subjects. Many antibacterial polymer or medicinal molecule are being designed from decades ago, some of them could kill the gram-positive types of bacteria but have limited effects on gram-negative bacteria, or vice versa due to the fact fundamental difference of two bacterial cell walls.

Recently researchers have developed broad-spectrum treatment to fight against both gram-negative and gram-positive types of bacteria, one of the novel methods is using some bio-compatible materials to trigger the Reactive oxygen species (ROS) generation from low concentration of H_2O_2, which was reported that has high antibacterial effects. However, high level of H_2O_2 or the poor biocompatibility materials could be toxic to the living forms.

Lysozyme is natural antimicrobial enzyme produced by animals that forms part of the innate immune system. Also, lysozyme is abundant in secretions including tears, saliva, and human milk. Large amounts of lysozyme can be found in egg white. Lysozyme is a glycoside hydrolase that catalyzes the hydrolysis of 1,4-betalinkages between N-acetylmuramic acid and N-acetyl-D-glucosamine residues in peptidoglycan, which is the major component of the gram-positive bacterial cell wall. So, lysozymes generally show better antibacterial activity to gram-positive

bacteria than gram-negative bacteria. Some work has been published to enhance the antibacterial activity of lysozyme with the aid of nano/micro size materials. The high surface area of nano/micromaterials can absorb more lysozyme and induce the enhancement of antibacterial activity.

Herein, we conjugated the lysozyme protein on the catalyst material PEG/Fe-LDH that can decompose hydrogen peroxide to hydroxyl radicals, and we found that the Lyso@PEG/Fe-LDH composite treatment has significant better effects than the separated treatments. We anticipated the enhancement of antibacterial effects rendering the lysozyme disturbs the bacterial cell walls, and the hydroxyl radical attacks on bacterial membranes, causing the synergistic effect on damaging bacteria.

4.2 Experimental

Synthesis of Nanoparticles: The PEG/Fe-LDH precursor were prepared as previously reported. Briefly, The $FeCl_2$ (0.2536 g, 2 mmol) and $AlCl_3 \cdot 6H_2O$ (0.2414 g, 1 mmol) were dissolved in degassed Milli-Q water, and then mixed with 6 mmol of NaOH with constant pH value under nitrogen atmosphere. Next, the 0.2 g of dual phosphonic acid-polyethylene glycol diblock copolymer (PEG) (molecular weight = 10 000 g mol^{-1}, degree of polymerization = 22) was added into the mixture, followed by hydrothermal treatment at 100 °C for 8 h. The LDH particles were obtained after 3-times centrifugation. After that, the PEG/Fe-LDH suspension was added to the lysozyme (2.56 mg/ml) in a dropwise manner under vigorous stirring and nitrogen for 2h.

Turbidity assay: mono-colony of gram-negative *(E. coli)* and gram-positive *(S. aureus)* bacteria was collected from agar plate and culture in 10 mL of fluid Luria−Bertani (LB) medium and keep shaking at 37 ºC overnight without any disruption. After the overnight culture, the bacterial suspension was diluted to 10^6 CFU/mL *via* pH-adjusted LB medium (containing 40 mM Tris-HCl). Then, samples (200 μg/mL of Lyso@PEG/Fe-LDH with 1 mM H_2O_2, 2.56 mg/mL lysozyme, 200 μg/mL PEG/Fe-LDH with 1 mM H_2O_2 and PBS) were added to the bacterial suspension and the mixture was shaking under 37 ºC, 180 rpm for 16 hrs. Finally, the suspension optical density was measured the absorbance at 600 nm light.

Minimum Inhibitory Concentration (MIC) Test: The minimum inhibitory concentrations (MICs) of lysozyme were determined *via* the broth microdilution method according to Clinical and Laboratory Standards Institute (CLSI) guidelines. Briefly, a single colony was cultured in 10 mL of Mueller-Hinton broth (MHB) at 37 °C with shaking at 180 rpm overnight. Subsequently, a subculture was prepared from the overnight culture by diluting 1:100 in 10 mL of MHB and allowed to grow to mid log phase; then, it was diluted to the appropriate concentration with pH adjusted MHB medium (containing 40 mM Tris-HCl) for the MIC test. A 2-fold dilution series of 100 μL of lysozyme solution in MHB was added into 96-well microplates followed by the addition of 100 μL of the subculture suspension. The final concentration of bacteria in each well was ca. 5×10^5 cells mL^{-1}. The plates were incubated at 37 °C for 20 h, and the absorbance at 600 nm was measured with a microtiter plate reader (FLUOstar Omega, BMG Labtech). MIC values were defined as the lowest concentration of

sample that showed no visible growth and inhibited cell growth by more than 90%. Positive controls without lysozyme and negative controls without bacteria were included.

Killing Studies: To evaluate the bactericidal activity of PEG-Fe/LDH with H_2O_2, *Escherichia coli (E. coli)* and *Staphylococcus aureus (S. aureus)* were chosen. A single colony of *E. coli* or *S. aureus* was cultured overnight in 10 mL of Luria−Bertani medium (LB 10) at 37 °C with shaking at 180 rpm. The overnight culture was diluted to appropriate concentration with pH adjusted LB medium (pH = 6). Then, the bacterial suspension was then aliquoted (1 mL per well) into tissue-culture treated 24-well plates (Costar, Corning). Each well was then added 200 μg/mL of PEG/Fe-LDH and pre-determined serial concentration of H_2O_2. The plates were incubated at 37 °C with shaking at 180 rpm in an orbital shaker that does not stop agitation when the door is opened (model OM11, Ratek, Boronia, Australia), for 1 h without any disruption. After incubation, free-floating cells in the supernatant were serially diluted in sterile PBS and plated onto LB agar plate. The numbers of colonies were counted, and CFU was calculated after 24 h of incubation at 37 °C. All assays included two replicates and were repeated in at least three independent experiments.

4.3 Results and Discussion

4.3.1 Characterization

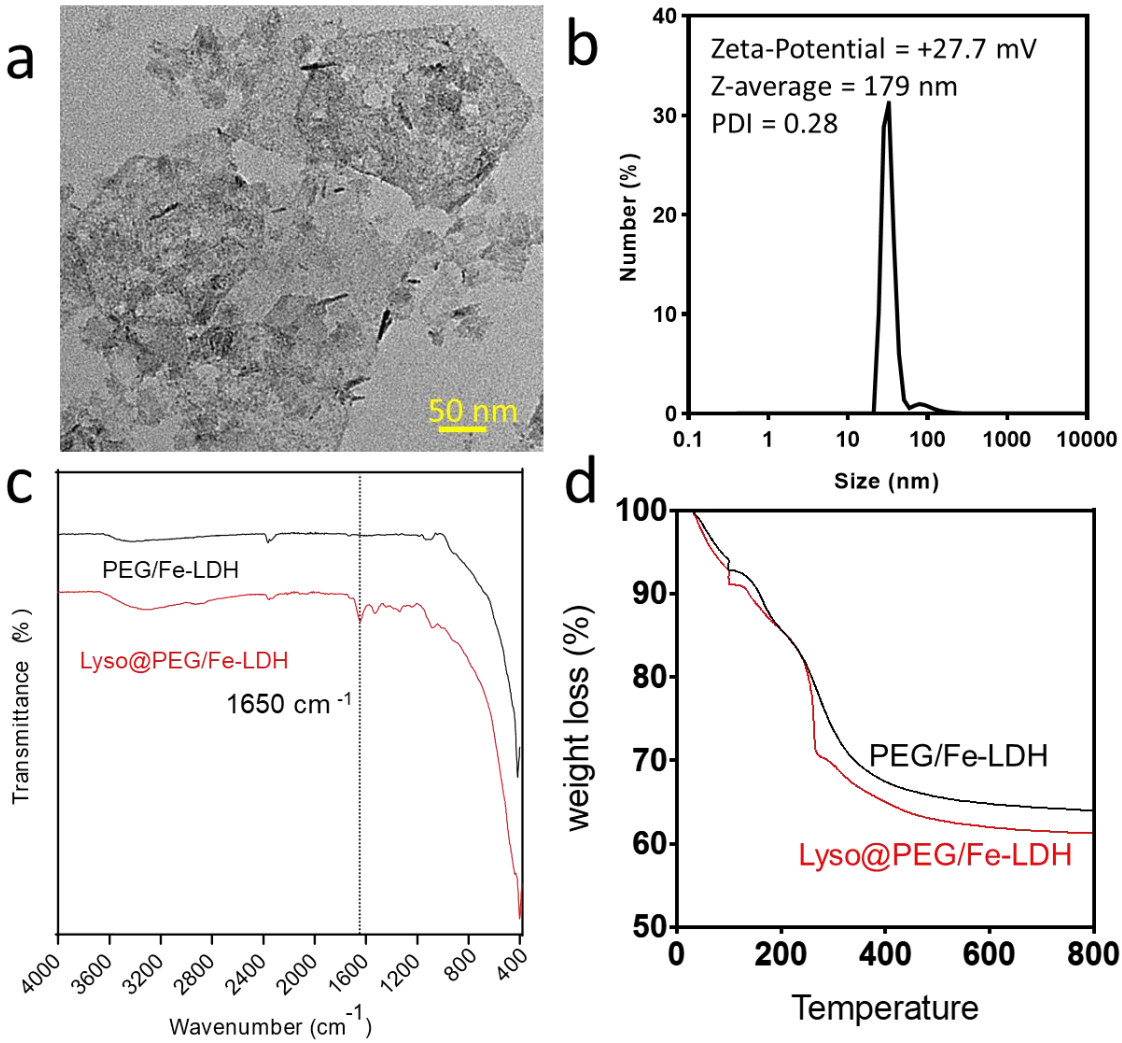

Figure 4.1. Phychemical properties of Lyso@PEG/Fe-LDH nanosheets. a) TEM image, b) hydrodynamic size distribution of Lyso@PEG/Fe-LDH, c) FTIR spectra and d) TGA curses of PEG/Fe-LDH & Lyso@PEG/Fe-LDH

The 2D antibacterial nanosheet (Lyso@PEG/Fe-LDH) was constructed by coprecipitating, alkaline and metal ions (Fe (II) & Al^{3+}) followed by hydrothermal aging, the anionic PEG (dual phosphonic acid–polyethylene glycol diblock copolymer) was added to control the nanosheet

growth. After that, a certain amount of lysozyme was loaded on PEG/Fe-LDH precursor. Transmission electron microscopy (TEM) image reveals that the PEG/Fe-LDH has the hexagonal shape with a lateral diameter around 200 nm (Figure 4.1a). DLS result indicating that Lyso@PEG/Fe-LDH has the hydrodynamic sizes circus 179 nm, slightly smaller than PEG/Fe-LDH (around 200 nm) (Figure 3.2f) while they are presenting in water (Figure 4.1b), with a PDI of 0.28. Judging from the Y-axis, it is worth noted that a large percentage of the particles were remain less than 100 nm, indicating after conjugating with lysozyme, the particles remain in nanoscale. In Fourier transform infrared (FTIR) spectra, stretching vibration form N-H amine from lysozyme molecules recorded at 1650 to 1580 cm^{-1} in the Lyso@PEG/Fe-LDH spectrum, while it was not observed in the PEG/Fe-LDH sample, suggesting that lysozyme was successfully attach on PEG/Fe-LDH nanosheet (Figure 4.1c). The weight ratio of lysozyme loaded-on PEG/Fe-LDH nanosheet was quantified to be 2.63% *via* thermal gravimetric analysis (TGA) (Figure 4.1d).

4.3.2 Antibacterial experiments

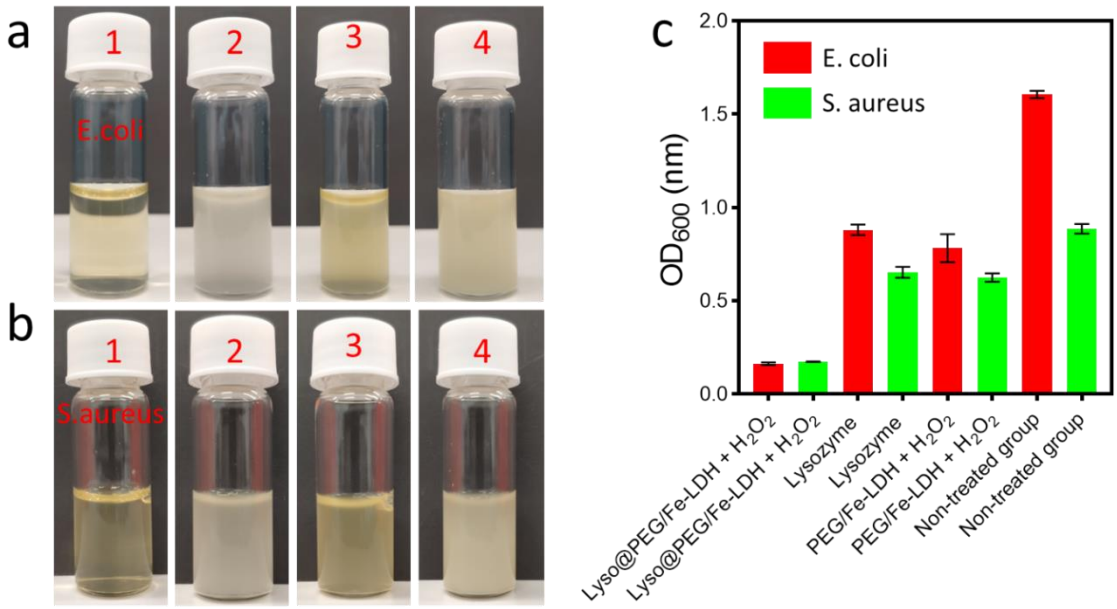

Figure 4.2. Turbidity Assay of a) *E. coli* and b) *S. aureus* and the corresponding OD_{600} values. (**1:** Lysozyme + PEG/Fe-LDH + H_2O_2, **2:** Lysozyme, **3:** PEG/Fe-LDH + H_2O_2, **4:** Non-treated group)

We tested the antibacterial activity of Lyso@PEG/Fe-LDH by the Luria−Bertani (LB) fluid medium turbidity assay. Two types of bacteria, gram-negative *Escherichia coli (E. coli)* and gram-positive *Staphylococcus aureus (S. aureus)* were chosen as microbial models to evaluate the antibacterial activity of Lyso@PEG/Fe-LDH. We collect single colony of *E. coli* or *S. aureus* from an agar coated plate in LB liquid media and cultured the bacteria alone as a control sample. Lysozyme (2.56 mg/mL), PEG/Fe-LDH (200 μg/mL) with 1mM H_2O_2 and Lyso@PEG/Fe-LDH with 1mM H_2O_2 (200 μg/mL, the interfacial concentrations of lysozyme are around 5.26 μg/mL) (Calculated from TGA results, 200 μg/mL x2.63% = 5.26 μg/mL) are added into the bacterial media. After culturing 16 h in a shaker at 37 °C 180 rpm, the tube containing Lyso@PEG/Fe-LDH remained transparent, indicating few *E. coli* and *S. aureus* proliferated. While the non-treated group became turbid, and the tube with lysozyme and PEG/Fe-LDH with 1mM H_2O_2 was translucent (Figure 4.2a, 2b) indicating two treatments also showed some but limited inhibiting ability. We further quantified the OD values of samples under 600 nm wavelength light (OD_{600}). The sample contained Lyso@PEG/Fe-LDH with H_2O_2 showed the lowest absorbance; PEG/Fe-LDH with H_2O_2 and lysozyme alone also present some antibacterial efficacy. Lysozyme alone and hydroxyl radical shown the inhibition effect on bacterial growth but not as effective as the Lyso@PEG/Fe-LDH composites. We also studied the Minimum inhibitory concentration (MIC) of lysozyme and the bacteria survival rate against the hydroxyl radical that generated *via* PEG/Fe-LDH catalyzed H_2O_2 decomposition. The MIC

results of lysozyme against *E. coli* that was around 10.24 mg/mL, and the concentration was even greater when it subjected on *S. aureus* (Table 1). The killing assay indicated that *the E. coli* and *S. aureus* have circus 35% and 85% survival rate after treated by PEG/Fe-LDH with 1mM H_2O_2 (Figure 4.3.) Together, these indicates two separated treatments could not reach an ideal efficiency of killing both gram-positive and gram-negative bacteria.

Table 1. MIC of lysozyme against *E. coli* and *S. aureus*

Bacteria/concentration(mg/mL)	10.24	5.12	2.56	1.28	6.4	3.2
E. coli	89.44	86.21	79.72	77.83	77.44	74.89
S. aureus	82.24	73.65	71.62	67.61	64.63	63.61

+

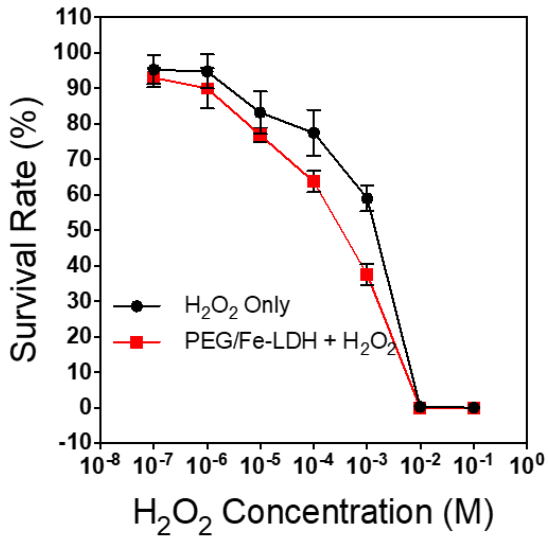

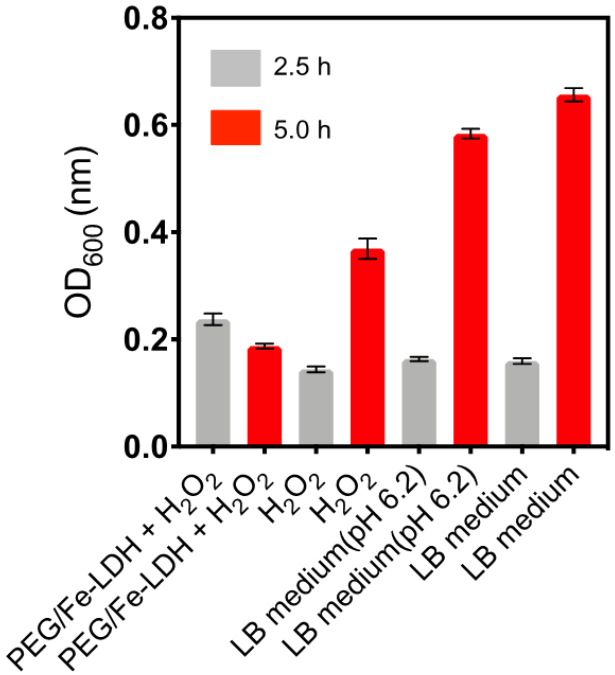

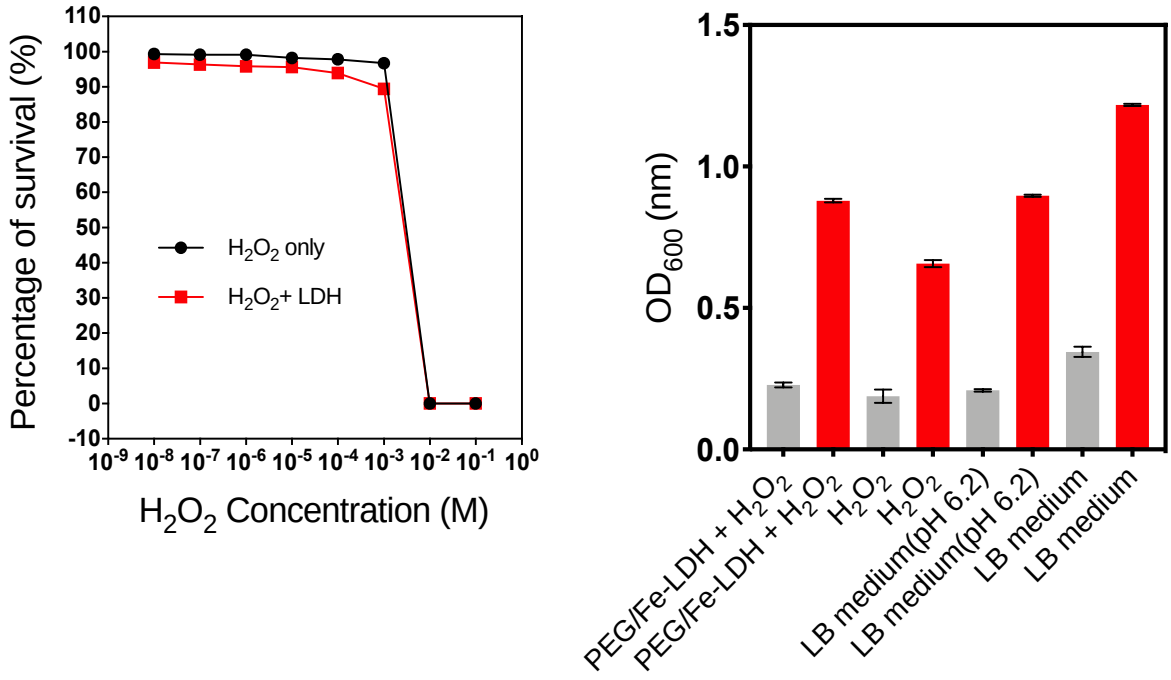

Figure 4.3. *E. coli* & *S. aureus* survival rate after treated with PEG/Fe-LDH (200 ug/mL) with different concentration under pH 6.2 for 60 mins; Right: *E. coli* & *S. aureus* OD600 values after treat with PEG/Fe-LDH (200 ug/mL) and 1mM H_2O_2 after 2.5 h (grey) and 5 h (red).

4.3.3 Bacterial Morphology

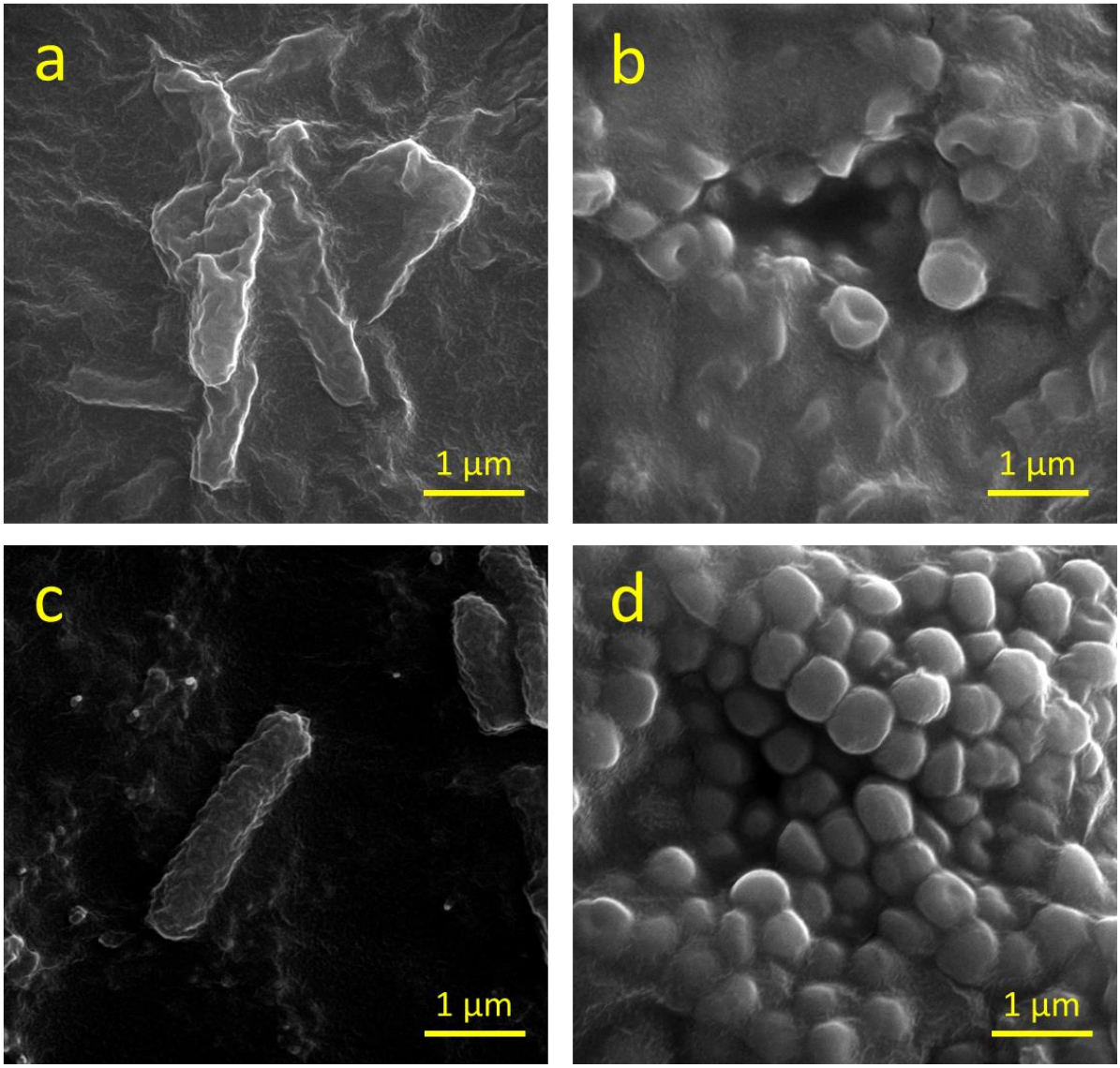

Figure 4.4. SEM images of a) *E. coli* treated with 200 µg/mL of PEG/Fe-LDH and 1mM of H_2O_2 b) non-treated *E. coli*; c) *S. aureus* treated with 200 µg/mL of PEG/Fe-LDH and 1mM of H_2O_2, d) non-treated *S. aureus*.

To investigate the changes of bacterial morphology induced by the antibacterial system, scanning electron microscope (SEM) was used to observe *E. coli* and *S. aureus* before and after the PEG/Fe-LDH treatment. As shown in Figure 4.4, *E. coli* cells treated just with PEG/Fe-

LDH (Figure 4.4a) with H_2O_2, the bacterial surface became rough and wrinkled since free radicals from H_2O_2 can oxidize the lipid membrane and destroy the bacterial membranes while the untreated *E. coli* (Figure 4.4c) and were typically rod-shaped, with smooth and intact cell walls. As for *S. aureus* cells, the results of SEM experiments were similar to that of *E. coli* cells (Figure 4.4b & 4.4d). Without the addition of PEG/Fe-LDH and H_2O_2, the *S. aureus* cells were spherical and smooth; in the presence of PEG/Fe-LDH and H_2O_2, *S. aureus* cells resulted to rough and damaged. From the ESR spectra, the hydroxyl radicals were proved to be generated in acidic environment by PEG/Fe-LDH catalyzing (Figure 4.5), while insignificant radicals were generated in the alkaline environment.

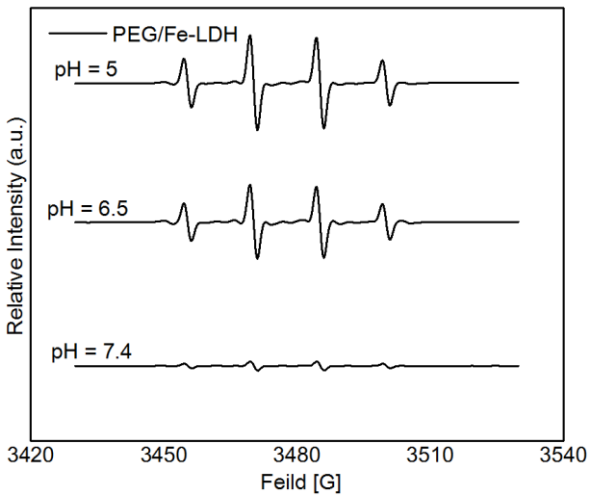

Figure 4.5. ESR spectra of PEG/Fe-LDH catalyzing hydroxyl radicals' generation.

4.4 Conclusion

In summary, an antibacterial system combining lysozyme and PEG/Fe-LDH with low dose of common medical reagent, H_2O_2, was designed. Due to the special layered structure of LDH, it provides the particles large surface area for catalyst activity, as well as the potential for loading medicinal molecules. In this work, we synthesize and characterize lysozyme conjugated with PEG/Fe-LDH, and discovered, while the single treatment of lysozyme or hydroxyl radical

against the microbial has limited efficacy, the combination of lysozyme and free hydroxyl radical treatment have greater effect on both gram-positive and gram-negative bacteria. Lyso@PEG/Fe-LDH could have broader application in antimicrobe due to their excellent biocompatibility and synergistic function with other components.

Chapter 5
Conclusions and Outlook

In this thesis work, a literature review has been presented regarding layered double hydroxides. Their unique structure, properties, synthesis methods, characterization techniques, and the potential uses of LDHs were discussed. Taking the advantages of high catalyzing ability of ferrous ions, Fe-LDH was successfully constructed. The drawback of the Fe-LDH was easily being oxidized and aggregated, which could significantly hinder its catalyzing ability. To avoid this drawback, numerous techniques has also proposed. This review enlightened the potential paths of modifying Fe-LDH, which were displayed in chapter 3 and chapter 4.

In chapter 3, the PEG/Fe-LDH catalyzing oxygen generation ability has been discussed. Detailly, PEG/Fe-LDH as nanomotor the anti-cancer therapy was presented. PEG has exfoliated the Fe-LDH to thin nanosheet, and they could efficiently generate oxygen from hydrogen peroxide as fuel to propel themselves. Based on the particle's movement trajectories, a directional movement was detected and studied. We attempted to load the doxorubicin as cargo for drug delivery toward cancer therapy. This unique property is worth to be further explored as they could fulfill targeting-delivery mission.

In addition to oxygen generation, in chapter 4, the ability of PEG/Fe-LDH catalyzing radicals generation was further investigated. In the acidic environment, the PEG/Fe-LDH tent to decompose hydrogen peroxide into hydroxyl and hydroperoxyl radicals. Based on this background, PEG/Fe-LDH antibacterial performance was tested. As we found that the radicals could only have antibacterial effects on gram-negative types of bacteria, we further coated

lysozyme onto PEG/Fe-LDH. After that, the nanocomposites could therefore fight against both gram-positive and gram-negative bacteria in a better efficacy than the lysozyme or PEG/Fe-LDH separated treatments. Further investigation could focus on anti-virus or any other microorganism.

Chapter 6 References

1. Gu, Z., J.J. Atherton, and Z.P. Xu, *Hierarchical layered double hydroxide nanocomposites: structure, synthesis and applications.* Chem Commun (Camb), 2015. **51**(15): p. 3024-36.

2. Zhao, Y., et al., *Layered Double Hydroxide Nanostructured Photocatalysts for Renewable Energy Production.* Advanced Energy Materials, 2016. **6**(6): p. 1501974.

3. Zubair, M., et al., *Recent progress in layered double hydroxides (LDH)-containing hybrids as adsorbents for water remediation.* Applied Clay Science, 2017. **143**: p. 279-292.

4. Cao, Z., et al., *2D layered double hydroxide nanoparticles: Recent progress toward preclinical/clinical Nanomedicine.* Small Methods, 2020. **4**(2): p. 1900343.

5. Wang, Q. and D. O'Hare, *Recent advances in the synthesis and application of layered double hydroxide (LDH) nanosheets.* Chem Rev, 2012. **112**(7): p. 4124-55.

6. Xu, S., et al., *Surface modification and dissolution behavior of Mg–Al hydrotalcite particles.* Journal of the Taiwan Institute of Chemical Engineers, 2015. **56**: p. 174-180.

7. Cui, P., et al., *Meter-scale fabrication of water-driven triboelectric nanogenerator based on in-situ grown layered double hydroxides through a bottom-up approach.* Nano Energy, 2020. **71**: p. 104646.

8. Mao, N., et al., *Exfoliation of layered double hydroxide solids into functional nanosheets.* Applied Clay Science, 2017. **144**: p. 60-78.

9. Xu, Z.P., et al., *Stable Suspension of Layered Double Hydroxide Nanoparticles in Aqueous Solution.* Journal of the American Chemical Society, 2006. **128**(1): p. 36-37.

10. Dresp, S., et al., *Efficient direct seawater electrolysers using selective alkaline NiFe-*

LDH as OER catalyst in asymmetric electrolyte feeds. Energy & Environmental Science, 2020. **13**(6): p. 1725-1729.

11. Wang, Y., et al., *A fully heterogeneous catalyst Br-LDH for the cycloaddition reactions of CO 2 with epoxides.* Chemical Communications, 2019. **55**(48): p. 6942-6945.
12. Yang, H., et al., *In situ growth of ultrathin Ni–Fe LDH nanosheets for high performance oxygen evolution reaction.* Inorganic Chemistry Frontiers, 2017. **4**(7): p. 1173-1181.
13. Wang, S., et al., *The catalytic degradation of nitrobenzene by the Cu–Co–Fe-LDH through activated oxygen under ambient conditions.* Dalton Transactions, 2020. **49**(13): p. 3999-4011.
14. Yu, I.K.M., et al., *Tuneable Functionalities in Layered Double Hydroxide Catalysts for Thermochemical Conversion of Biomass-Derived Glucose to Fructose.* Chemical Engineering Journal, 2019.
15. Dou, Y., et al., *TiO2@ Layered double hydroxide core–shell nanospheres with largely enhanced photocatalytic activity toward O2 generation.* Advanced Functional Materials, 2015. **25**(15): p. 2243-2249.
16. Kremer, M.L., *Mechanism of the Fenton reaction. Evidence for a new intermediate.* Physical Chemistry Chemical Physics, 1999. **1**(15): p. 3595-3605.
17. Chen, Z., et al., *Dual Enzyme-like Activities of Iron Oxide Nanoparticles and Their Implication for Diminishing Cytotoxicity.* ACS Nano, 2012. **6**(5): p. 4001-4012.
18. Perez-Benito, J.F., *Iron(III)−Hydrogen Peroxide Reaction: Kinetic Evidence of a Hydroxyl-Mediated Chain Mechanism.* The Journal of Physical Chemistry A, 2004. **108**(22): p. 4853-4858.

19. Qu, J., et al., *Applications of mechanochemically prepared layered double hydroxides as adsorbents and catalysts: A mini-review.* Nanomaterials, 2019. **9**(1): p. 80.

20. Liu, P.F., et al., *Defect-rich ultrathin cobalt–iron layered double hydroxide for electrochemical overall water splitting.* ACS applied materials & interfaces, 2016. **8**(50): p. 34474-34481.

21. Karmali, P.P. and D. Simberg, *Interactions of nanoparticles with plasma proteins: implication on clearance and toxicity of drug delivery systems.* Expert Opin Drug Deliv, 2011. **8**(3): p. 343-57.

22. Yu, J., et al., *Preparation of two dimensional layered double hydroxide nanosheets and their applications.* Chemical Society Reviews, 2017. **46**(19): p. 5950-5974.

23. Wilson Jr, O., et al., *Surface and interfacial properties of polymer-intercalated layered double hydroxide nanocomposites.* Applied Clay Science, 1999. **15**(1-2): p. 265-279.

24. Gu, Z., et al., *Pre-coating layered double hydroxide nanoparticles with albumin to improve colloidal stability and cellular uptake.* Journal of Materials Chemistry B, 2015. **3**(16): p. 3331-3339.

25. Cao, Z., et al., *Enhanced colloidal stability and protein resistance of layered double hydroxide nanoparticles with phosphonic acid-terminated PEG coating for drug delivery.* J Colloid Interface Sci, 2018. **521**: p. 242-251.

26. Islam, M. and R. Patel, *Synthesis and physicochemical characterization of Zn/Al chloride layered double hydroxide and evaluation of its nitrate removal efficiency.* Desalination, 2010. **256**(1-3): p. 120-128.

27. Allegra, G. and G. Ronca, *Crystal powder statistics. II. Line profiles in diffraction*

spectra of identical crystals and of Gaussian samples. Crystal size distributions. Acta Crystallographica Section A: Crystal Physics, Diffraction, Theoretical and General Crystallography, 1978. **34**(6): p. 1006-1013.

28. Roy, R. and E.F. Osborn, *The system MgO-Al 2 O 3-H 2 O and influence of carbonate and nitrate ions on the phase equilibria.* American Journal of Science, 1953. **251**(5): p. 337-361.

29. Allmann, R.v., *Doppelschichtstrukturen mit brucitahnlichen Schichtionen [Me (II) _< 1-x> Me (III) _x (OH) _2]^< x+.* Chimia, 1970. **24**: p. 99-108.

30. Zhai, R.-S., et al., *Polymeric fullerene oxide films produced by decomposition of hexanitro [60] fullerene.* Carbon, 2004. **42**(2): p. 395-403.

31. Ding, P. and B. Qu, *Synthesis and characterization of exfoliated polystyrene/ZnAl layered double hydroxide nanocomposite via emulsion polymerization.* J Colloid Interface Sci, 2005. **291**(1): p. 13-8.

32. Kloprogge, J.T., L. Hickey, and R.L. Frost, *The effect of varying synthesis conditions on zinc chromium hydrotalcite: a spectroscopic study.* Materials Chemistry and Physics, 2005. **89**(1): p. 99-109.

33. Hakeem, A., et al., *Facile synthesis of pH-responsive doxorubicin-loaded layered double hydroxide for efficient cancer therapy.* Journal of Materials Chemistry B, 2018. **6**(36): p. 5768-5774.

34. Xu, Z.P., et al., *Dispersion and Size Control of Layered Double Hydroxide Nanoparticles in Aqueous Solutions.* The Journal of Physical Chemistry B, 2006. **110**(34): p. 16923-16929.

35. Cao, Z., et al., *Biodegradable 2D Fe–Al Hydroxide for Nanocatalytic Tumor-Dynamic Therapy with Tumor Specificity.* Advanced Science, 2018. **5**(11): p. 1801155.

36. Xie, J., et al., *Controlled PEGylation of Monodisperse Fe3O4 Nanoparticles for Reduced Non-Specific Uptake by Macrophage Cells.* Advanced Materials, 2007. **19**(20): p. 3163-3166.

37. Choy, J.H., et al., *Inorganic layered double hydroxides as nonviral vectors.* Angewandte Chemie International Edition, 2000. **39**(22): p. 4041-4045.

38. Oh, J.-M., et al., *Cellular Uptake Mechanism of an Inorganic Nanovehicle and Its Drug Conjugates: Enhanced Efficacy Due To Clathrin-Mediated Endocytosis.* Bioconjugate Chemistry, 2006. **17**(6): p. 1411-1417.

39. Swadling, J.B., et al., *Influence of surface chemistry and charge on mineral-RNA interactions.* Langmuir, 2013. **29**(5): p. 1573-83.

40. Xiao, G.F., et al., *Facile Preparation of Modifying Layered Double Hydroxide Nanoparticles for Drug Delivery.* J Nanosci Nanotechnol, 2018. **18**(8): p. 5256-5265.

41. Gu, Z., et al., *In Vitro Sustained Release of LMWH from MgAl-layered Double Hydroxide Nanohybrids.* Chemistry of Materials, 2008. **20**(11): p. 3715-3722.

42. Yang, J.-H., et al., *New Inorganic-Based Drug Delivery System of Indole-3-Acetic Acid-Layered Metal Hydroxide Nanohybrids with Controlled Release Rate.* Chemistry of Materials, 2007. **19**(10): p. 2679-2685.

43. Huang, G., et al., *Manganese-iron layered double hydroxide: a theranostic nanoplatform with pH-responsive MRI contrast enhancement and drug release.* Journal of Materials Chemistry B, 2017. **5**(20): p. 3629-3633.

44. Oh, J.M., et al., *Inorganic metal hydroxide nanoparticles for targeted cellular uptake through clathrin-mediated endocytosis.* Chemistry–An Asian Journal, 2009. **4**(1): p. 67-73.

45. Li, S., et al., *Cellular uptake and gene delivery using layered double hydroxide nanoparticles.* J. Mater. Chem. B, 2013. **1**(1): p. 61-68.

46. Dai, B., et al., *Programmable artificial phototactic microswimmer.* Nat Nanotechnol, 2016. **11**(12): p. 1087-1092.

47. Shao, J., et al., *Chemotaxis-Guided Hybrid Neutrophil Micromotors for Targeted Drug Transport.* Angew Chem Int Ed Engl, 2017. **56**(42): p. 12935-12939.

48. Loosley, A.J., et al., *Describing directional cell migration with a characteristic directionality time.* PloS one, 2015. **10**(5): p. e0127425.

49. McCutcheon, M., *Chemotaxis in leukocytes.* Physiological reviews, 1946. **26**(3): p. 319-336.

50. Gao, S., et al., *Superassembled Biocatalytic Porous Framework Micromotors with Reversible and Sensitive pH-Speed Regulation at Ultralow Physiological H 2 O 2 Concentration.* Advanced Functional Materials, 2019. **29**(18): p. 1808900.

51. Guo, Z., et al., *Biocatalytic self-propelled submarine-like metal-organic framework microparticles with pH-triggered buoyancy control for directional vertical motion.* Materials Today, 2019.

52. Wang, W., et al., *Understanding the efficiency of autonomous nano- and microscale motors.* J Am Chem Soc, 2013. **135**(28): p. 10557-65.

53. Howse, J.R., et al., *Self-Motile Colloidal Particles: From Directed Propulsion to*

Random Walk. Physical Review Letters, 2007. **99**(4).

54. Li, L., et al., *A unified model of drag force for bubble-propelled catalytic micro/nano-motors with different geometries in low Reynolds number flows.* Journal of Applied Physics, 2015. **117**(10).

55. Mei, L., et al., *Two-dimensional nanomaterials beyond graphene for antibacterial applications: current progress and future perspectives.* Theranostics, 2020. **10**(2): p. 757-781.

56. Alimohammadi, F., et al., *Antimicrobial properties of 2D MnO2 and MoS2 nanomaterials vertically aligned on graphene materials and Ti3C2 MXene.* Langmuir, 2018. **34**(24): p. 7192-7200.

57. Sun, H., et al., *Graphene quantum dots-band-aids used for wound disinfection.* ACS nano, 2014. **8**(6): p. 6202-6210.

58. Xu, Z., et al., *Converting organosulfur compounds to inorganic polysulfides against resistant bacterial infections.* Nature communications, 2018. **9**(1): p. 1-13.

59. Wang, J. and W. Gao, *Nano/microscale motors: biomedical opportunities and challenges.* ACS nano, 2012. **6**(7): p. 5745-5751.

60. Karshalev, E., B. Esteban-Fernandez de Avila, and J. Wang, *Micromotors for "Chemistry-on-the-Fly".* J Am Chem Soc, 2018. **140**(11): p. 3810-3820.

61. Li, J., et al., *Micro/Nanorobots for Biomedicine: Delivery, Surgery, Sensing, and Detoxification.* Sci Robot, 2017. **2**(4).

62. Campuzano, S., et al., *Nano/microvehicles for efficient delivery and (bio)sensing at the cellular level.* Chem Sci, 2017. **8**(10): p. 6750-6763.

63. Gao, W. and J. Wang, *Synthetic micro/nanomotors in drug delivery.* Nanoscale, 2014. **6**(18): p. 10486-94.

64. Esteban-Fernandez de Avila, B., et al., *Cell-Like Micromotors.* Acc Chem Res, 2018. **51**(9): p. 1901-1910.

65. Wei, X., et al., *Biomimetic Micromotor Enables Active Delivery of Antigens for Oral Vaccination.* Nano Lett, 2019. **19**(3): p. 1914-1921.

66. Karshalev, E., et al., *Micromotor Pills as a Dynamic Oral Delivery Platform.* ACS Nano, 2018. **12**(8): p. 8397-8405.

67. Tu, Y., F. Peng, and D.A. Wilson, *Motion Manipulation of Micro- and Nanomotors.* Adv Mater, 2017. **29**(39).

68. Wang, J. and K.M. Manesh, *Motion control at the nanoscale.* Small, 2010. **6**(3): p. 338-45.

69. Sanchez, S., L. Soler, and J. Katuri, *Chemically powered micro- and nanomotors.* Angew Chem Int Ed Engl, 2015. **54**(5): p. 1414-44.

70. Wang, J., *Biomolecule-functionalized nanowires: from nanosensors to nanocarriers.* Chemphyschem, 2009. **10**(11): p. 1748-55.

71. Ma, X., et al., *Enzyme-Powered Hollow Mesoporous Janus Nanomotors.* Nano Lett, 2015. **15**(10): p. 7043-50.

72. Sattayasamitsathit, S., et al., *Dual-enzyme natural motors incorporating decontamination and propulsion capabilities.* RSC Adv., 2014. **4**(52): p. 27565-27570.

73. Kumar, A. and Q. Xu, *Two-Dimensional Layered Materials as Catalyst Supports.* ChemNanoMat, 2018. **4**(1): p. 28-40.

74. Li, M., Z. Luo, and Y. Zhao, *Recent advancements in 2D nanomaterials for cancer therapy.* Science China Chemistry, 2018. **61**(10): p. 1214-1226.

75. Li, B.L., et al., *Engineered functionalized 2D nanoarchitectures for stimuli-responsive drug delivery.* Materials Horizons, 2020.

76. Liu, Z., et al., *Synthesis, Anion Exchange, and Delamination of Co−Al Layered Double Hydroxide: Assembly of the Exfoliated Nanosheet/Polyanion Composite Films and Magneto-Optical Studies.* Journal of the American Chemical Society, 2006. **128**(14): p. 4872-4880.

77. A. Ali, N., *Barrier, Mechanical and Thermal of Polyvinyl Alchol/Microcrystalline Cellouse Composites in Packaging Application.* American Journal of Physics and Applications, 2017. **5**(4).

78. Orozco, J., et al., *Bubble-Propelled Micromotors for Enhanced Transport of Passive Tracers.* Langmuir, 2014. **30**(18): p. 5082-5087.

79. Ma, X., K. Hahn, and S. Sanchez, *Catalytic Mesoporous Janus Nanomotors for Active Cargo Delivery.* 2015. **137**(15): p. 4976-4979.

80. Peng, F., et al., *Self-Guided Supramolecular Cargo-Loaded Nanomotors with Chemotactic Behavior towards Cells.* Angewandte Chemie International Edition, 2015. **54**(40): p. 11662-11665.

81. Breunig, M., S. Bauer, and A. Goepferich, *Polymers and nanoparticles: intelligent tools for intracellular targeting?* Eur J Pharm Biopharm, 2008. **68**(1): p. 112-28.

82. Derfus, A.M., W.C.W. Chan, and S.N. Bhatia, *Intracellular Delivery of Quantum Dots for Live Cell Labeling and Organelle Tracking.* Advanced Materials, 2004. **16**(12): p.

961-966.

83. Duan, H. and S. Nie, *Cell-penetrating quantum dots based on multivalent and endosome-disrupting surface coatings.* Journal of the American Chemical Society, 2007. **129**(11): p. 3333-3338.

84. Xu, Z.P., et al., *Inorganic nanoparticles as carriers for efficient cellular delivery.* Chemical Engineering Science, 2006. **61**(3): p. 1027-1040.